

# Large impact of extreme precipitation on projected blue–green water partitioning

Simon P. Heselschwerdt<sup>1,2</sup>, Thorsten Wagener<sup>2</sup>, Lan Wang-Erlandsson<sup>3,4,5,6</sup>, Anna M. Ukkola<sup>7,8</sup>, Yannis Markonis<sup>9</sup>, Yuting Yang<sup>10,11</sup>, and Peter Greve<sup>1</sup>

<sup>1</sup>Climate Service Center Germany (GERICS), Helmholtz-Zentrum Hereon, Hamburg, Germany

<sup>2</sup>Institute of Environmental Science and Geography, University of Potsdam, Potsdam, Germany

<sup>3</sup>Stockholm Resilience Centre, Stockholm University, Stockholm, Sweden

<sup>4</sup>Bolin Centre for Climate Research, Stockholm University, Stockholm, Sweden

<sup>5</sup>Anthropocene Laboratory, The Royal Swedish Academy of Sciences, Stockholm, Sweden

<sup>6</sup>Potsdam Institute for Climate Impact Research (PIK), Member of the Leibniz Association, Potsdam, Germany

<sup>7</sup>ARC Centre of Excellence for Climate Extremes, University of New South Wales, Sydney, NSW, Australia

<sup>8</sup>Climate Change Research Centre, University of New South Wales, Sydney, NSW, Australia

<sup>9</sup>Department of Water Resources and Environmental Modeling, Faculty of Environmental Sciences, Czech University of Life Sciences Prague, Praha - Suchbát, Czech Republic

<sup>10</sup>State Key Laboratory of Hydrosphere Science and Engineering, Department of Hydraulic Engineering, Tsinghua University, Beijing, China

<sup>11</sup>Key Laboratory of Hydrosphere Sciences of the Ministry of Water Resources, Beijing, China

**Correspondence:** Simon P. Heselschwerdt (simon.heselschwerdt@hereon.de)

**Abstract.** Precipitation partitioning into blue (runoff) and green water (transpiration) flows is a fundamental hydroecological process shaping freshwater availability across vegetated and hydrologically active land areas. This partitioning is determined by interactions among climatic conditions, land surface characteristics, and vegetation dynamics, which change with rising temperatures and CO<sub>2</sub> concentrations. Yet, future global shifts in blue–green water partitioning, their controlling factors, and their broader implications remain uncertain. We address this knowledge gap using Earth system model simulations and define the Blue–Green Water Share (BGWS) metric to quantify changes in the relative partitioning of precipitation into runoff and transpiration. Here, we show that increases in extreme five-day precipitation are most strongly associated with future BGWS shifts, favouring larger blue water shares. This effect is independent of mean precipitation increases and occurs under both drying and wetting conditions. Additionally, increases in leaf area index tend to favour larger green water shares and counteract the blueward influence of stronger precipitation extremes. Our results provide a process-based perspective on projected blue–green water partitioning and its hydroecological implications.

## 1 Introduction

Ongoing anthropogenic climate change and other human interventions are reshaping the terrestrial water cycle and altering water availability globally (Wada et al., 2011; Greve et al., 2014; Milly and Dunne, 2016; Wada et al., 2016). These changes affect not only how much precipitation reaches the land surface, but also how that precipitation is partitioned among terrestrial water pathways. This matters because the same amount of precipitation can be divided into different shares of runoff, soil

moisture, evaporation, and transpiration. This partitioning affects water availability in rivers, reservoirs, and aquifers, as well as ecosystems and land–atmosphere interactions (Falkenmark, 2013; Falkenmark et al., 2019; Gleeson et al., 2020). Observations and Earth system models (ESMs) show that major land-water fluxes and stores are already changing in their amount, timing, and spatial distribution (Yang et al., 2023; Zaitchik et al., 2023; Gudmundsson et al., 2026). Understanding future water availability therefore requires understanding not only changes in precipitation itself, but also changes in how precipitation is partitioned at the land surface.

To interpret precipitation partitioning in terms of its relevance for ecosystems and human water use, we use the blue–green water paradigm (Falkenmark, 1995; Falkenmark and Rockström, 2006). In this framework, blue water stores refer to water stored in lakes, reservoirs, and aquifers, while blue water flows include runoff; together, these stores and flows support drinking water supply, irrigation, industrial use, and freshwater ecosystems (Falkenmark et al., 2019; Gleeson et al., 2020). Green water stores refer to soil moisture in the unsaturated zone, which supports vegetation growth and terrestrial productivity and is returned to the atmosphere through green water flows, including transpiration and evaporation (Rockström and Gordon, 2001; Falkenmark et al., 2019; Gleeson et al., 2020). Because blue and green water describe different forms and pathways of water availability, this framework complements standard variable-based hydrology by linking hydrological partitioning to its different roles for ecosystems and human water use.

We refer to the partitioning of precipitation into runoff and transpiration as blue–green water partitioning. Focusing on transpiration is useful because it captures a key pathway of plant water use, whereas metrics based on evapotranspiration (ET) or the complement of the runoff coefficient ( $1 - RC$ ) describe broader water-loss or non-runoff signals and do not isolate vegetation-mediated water use (Lawrence et al., 2007; Denissen et al., 2022; Bouaziz et al., 2022). Better understanding how precipitation is partitioned between runoff and transpiration is therefore important for interpreting shifts between runoff-related blue water availability and vegetation-mediated green water use.

Under climate change, this blue–green water partitioning is expected to shift because the climatic and hydroecological controls on runoff and transpiration are changing at the same time. Rising  $CO_2$  can reduce stomatal conductance and alter plant water-use efficiency (WUE), while changes in vegetation biomass can modify terrestrial water use and runoff responses (Leakey et al., 2009; Swann et al., 2016; Ukkola et al., 2016; Zhu et al., 2016; Mankin et al., 2018). At the same time, changes in atmospheric demand, soil moisture, and precipitation characteristics, including rainfall intensity and seasonality, can alter the balance between infiltration, storage, runoff generation, and transpiration (Donat et al., 2016; Skinner et al., 2017; Yin et al., 2018; Tabari, 2020; Scheff et al., 2022). Future changes in blue–green water partitioning therefore reflect interacting changes in climate and vegetation rather than changes in precipitation alone.

A growing body of work has already examined related aspects of precipitation partitioning. Studies of drought and climate change show that runoff and ET or transpiration can respond differently, with blue water flows in some regions declining more strongly than green water flows (Ukkola et al., 2016; Orth and Destouni, 2018). ESM analyses further show that vegetation change can reduce runoff across large parts of vegetated land, including in regions where precipitation increases (Mankin et al., 2018, 2019). Other studies have analysed related forms of terrestrial water partitioning at regional to global scales and highlighted the roles of hydrologic setting, catchment characteristics, rainfall intensity, land-surface processes and land use in

shaping how precipitation is divided between runoff, storage, and ecosystem water use (Weiskel et al., 2014; Eekhout et al., 2018; Yang et al., 2018; Scheff et al., 2022; Althoff and Destouni, 2023). Together, these studies have improved understanding of individual water fluxes, specific processes, and regional partitioning behaviour. However, less is known about the projected  
55 global patterns of runoff–transpiration partitioning across vegetated land areas and the factors associated with the spatial patterns of these changes.

This study aims to assess where future changes favour blue or green water pathways and which climatic and hydroecological changes are associated with these shifts. To do so, we define the Blue–Green Water Share (BGWS), a metric that quantifies the relative partitioning of precipitation into runoff and transpiration. We analyse the historical distribution of BGWS (1985–  
60 2014) and its projected changes under the SSP3–7.0 scenario (2071–2100 minus 1985–2014) using an ensemble of 12 ESMs participating in the Coupled Model Intercomparison Project Phase 6 (CMIP6; Eyring et al., 2016; Table S1). We then relate changes in BGWS to changes in mean and extreme precipitation, atmospheric water demand and cloud cover, soil moisture, and vegetation properties. Finally, we examine how BGWS changes co-occur with absolute changes in runoff and transpiration to provide a process-based interpretation of future changes in blue and green water availability and to discuss their implications  
65 in a warming, CO<sub>2</sub>-enriched world.

## 2 Data and methods

### 2.1 Earth system model data

We use output from 12 CMIP6 ESMs for both the historical experiment and the SSP3-7.0 scenario (Eyring et al., 2016; Table S1). SSP3-7.0 represents a regional rivalry pathway (Shared Socioeconomic Pathway 3) with a radiative forcing of  
70  $7 \text{ Wm}^{-2}$  by 2100 (Representative Concentration Pathway 7.0; Fujimori et al., 2017; Riahi et al., 2017). We select SSP3-7.0 because the warmest scenario, SSP5-8.5, is unlikely to be realised under current and projected emission trajectories (Hausfather and Peters, 2020). SSP3-7.0, as the second-highest emission scenario, is therefore particularly relevant for current climate impact assessments. However, we acknowledge that hydroecological responses are scenario-dependent (Yang et al., 2018). Given the impact focus of our analysis, we prioritise a scenario whose coupled forcings are more directly policy-relevant  
75 outcomes than idealised experiments.

The ESMs are selected to provide the variables required to compute the BGWS metric (Sect. 2.4) and the climatic and hydroecological variables used in the subsequent analyses (Sect. 2.5). Additionally, only models with time-varying leaf area index (LAI) were considered (Table S1). For each model, we select the ensemble member with the lowest available indices along the CMIP6 ensemble axes ("ripf": realisation, initialisation, physics and forcing; member IDs in Table S1). This approach  
80 ensures that each model contributes equally to the analysis and avoids over-representing models with a larger number of ensemble members.

## 2.2 Observation-based and reanalysis datasets

To evaluate the performance of the selected CMIP6 models in representing the BGWS, we compare the ESM results against observation-based and reanalysis datasets. Specifically, we compute the BGWS from GPCP precipitation (Schneider et al., 2022), G-RUN runoff (Ghiggi et al., 2019), and GLEAM transpiration (Miralles et al., 2011), providing an observation-based reference for model evaluation. These datasets are derived using different methodologies: GPCP is a gauge-based precipitation dataset, G-RUN reconstructs global runoff using a machine-learning approach trained on streamflow observations, and GLEAM is a hybrid observation–model product that estimates land-surface evaporation and transpiration from satellite-based data. Thus, these reference datasets are not equally direct observations and, due to their independent origins, are not fully consistent with one another or with a closed global water balance (Huang et al., 2025). To account for this, we also use ERA5-Land, a physically consistent reanalysis dataset providing all required variables from a single modelling framework (Muñoz-Sabater et al., 2021). However, reanalysis data are not direct observations and inherit uncertainties from model physics, model parametrisations and input data quality. While ERA5-Land offers a spatially and temporally coherent dataset, its ability to accurately represent long-term hydrological changes remains uncertain (Dutta and Markonis, 2024). We therefore use these global-scale gridded datasets as a first-order consistency check of ESM simulated BGWS patterns, rather than as a full benchmarking of ESM skill. In addition to comparing climatological BGWS fields, we also assess whether the ensemble mean reproduces observed changes in BGWS over the recent historical period. For this purpose, we compare BGWS changes between 1985–1999 and 2000–2014 in the CMIP6 ensemble mean and the reference datasets.

## 2.3 Data preprocessing and multi-model ensemble

To enable spatial comparison across models and datasets, we regrid all fields to a common  $1^\circ \times 1^\circ$  latitude–longitude grid using conservative interpolation. After regridding, we compute 30-year climatological means for a historical period (1985–2014) and a far-future period (2071–2100). Future-minus-historical changes are then calculated for all variables used in the subsequent analyses.

We apply a fixed historical mask derived from the ensemble mean over 1985–2014. The mask restricts the analysis to vegetated and hydrologically active land areas where the subsequent runoff–transpiration partitioning analysis is meaningful. Grid cells are retained only where mean precipitation exceeds  $0.05 \text{ mm day}^{-1}$ , mean runoff exceeds  $0.005 \text{ mm day}^{-1}$ , mean transpiration exceeds  $0.005 \text{ mm day}^{-1}$ , and mean LAI exceeds  $0.3 \text{ m}^2 \text{ m}^{-2}$ . These thresholds are deliberately low screening thresholds rather than hydroclimatic regime definitions. They exclude grid cells with very small water inputs, negligible runoff or transpiration, or sparse vegetation. The same mask is applied consistently to all historical fields, future changes, and reference datasets.

We employ an unweighted multi-model ensemble (hereafter referred to as the ensemble mean) to mitigate uncertainties associated with individual model biases and initial-condition variability. For each model, climatological means and changes are first computed at the model level and then averaged across models to obtain the ensemble mean. This ordering ensures that ensemble statistics reflect individual model responses before averaging. We do not apply performance-based weighting,

115 as our objective is to assess broad climate impacts rather than to optimise the ensemble for a specific variable. Spatial means are always calculated as area-weighted averages to account for the convergence of meridians with latitude. Each grid cell is weighted by the cosine of its latitude,  $\cos(\varphi)$ , where  $\varphi$  denotes latitude.

## 2.4 Blue–Green Water Share

In this study, we analyse blue–green water partitioning using precipitation ( $P$ ;  $\text{mm day}^{-1}$ ) as the incoming water supply, runoff ( $R$ ;  $\text{mm day}^{-1}$ ) as blue water flow and transpiration ( $E_t$ ;  $\text{mm day}^{-1}$ ) as the vegetation-mediated green water flow in vegetated and hydrologically active land areas. We focus on transpiration because it represents the direct vegetation water-use response, whereas non-transpirational evaporation may respond differently to climate change than vegetation-mediated water use (Lawrence et al., 2007). This distinction matters because total ET can reflect offsetting changes in its components. For example, transpiration can decrease while soil evaporation increases, so the ET response emerges from opposing biological and physical processes (Berg and Sheffield, 2019). Using ET instead of transpiration would therefore address a different question, namely runoff versus total evaporative loss rather than runoff versus vegetation-mediated water use (Denissen et al., 2022).

We introduce BGWS as a flow-based partitioning metric for runoff and transpiration rather than as a complete representation of all blue and green water or water-balance components. BGWS thus does not represent total green water flow, but specifically the vegetation-mediated component of green water use captured by transpiration. The historical mask defined in Sect. 2.3 ensures that the metric is evaluated only in regions where this transpiration-based interpretation is meaningful.

We define the BGWS metric as:

$$\text{BGWS} = \frac{R - E_t}{P} \times 100, \quad (1)$$

which is dimensionless and expressed in percent. Positive BGWS values indicate that a larger share of precipitation is partitioned towards runoff, whereas negative BGWS values indicate that a larger share is partitioned towards transpiration.

135 BGWS is therefore complementary to existing partitioning metrics. Relative to the blue water trade-off (BWT) metric used by Mankin et al. (2018, 2019), BGWS contrasts runoff directly with transpiration, does not include interception or storage terms, and reports the result as a normalised share of precipitation. Thus, interception-driven canopy effects are not represented explicitly by BGWS. For assessing vegetation-mediated green water use, however, transpiration as a direct ESM output is useful because it provides an immediate indicator of plant water use.

140 We focus on water fluxes rather than water stores because hydrological fluxes are more consistently available and more directly comparable across the selected CMIP6 ESMs. Moreover, on multi-decadal timescales (here, 30-year means), storage changes tend to be small relative to fluxes, as many catchments approach a near-steady state within this period (Han et al., 2020). Neglecting storage terms therefore provides a pragmatic and interpretable framework for large-scale analysis, although this simplification remains a limitation and an avenue for future research.

145 Changes in BGWS, denoted as  $\Delta\text{BGWS}$ , indicate shifts in blue–green water partitioning and are calculated as

$$\Delta\text{BGWS} = \text{BGWS}_{\text{Future}} - \text{BGWS}_{\text{Historical}}. \quad (2)$$

A positive  $\Delta\text{BGWS}$  reflects an increasing partitioning towards blue water flow, whereas a negative  $\Delta\text{BGWS}$  indicates an increasing partitioning towards green water flow. Although  $\Delta\text{BGWS}$  does not directly measure absolute changes in all blue and green water components, it provides a clear measure of the changing trade-off between runoff and transpiration.

To complement the transpiration-based analysis, we also compute non-transpirational evaporation  $E_{\text{nt}}$  as the difference  
 150 between ET and transpiration  $E_t$ ,

$$E_{\text{nt}} = \text{ET} - E_t. \quad (3)$$

This quantity represents non-transpirational evaporation, including soil evaporation, interception evaporation, and other non-transpirational components as represented in each dataset. We do not use CMIP6 component evaporation variables directly because key components (e.g. *evspsblsoi*) are unavailable for many models.

## 2.5 Climatic and hydroecological variables

155 We analyse both the historical 30-year climatological means and the future-minus-historical changes in selected climatic and hydroecological variables associated with the distribution and shifts in blue–green water partitioning. The selected variables are mean precipitation ( $P$ ;  $\text{mm day}^{-1}$ ), precipitation seasonality ( $P_{\text{seas}}$ ;  $\text{mm day}^{-1}$ ), annual maximum consecutive five-day precipitation (RX5day;  $\text{mm}$ ), surface soil moisture ( $\text{SM}_{\text{surf}}$ ;  $\text{mm}$ ), leaf area index (LAI;  $\text{m}^2 \text{m}^{-2}$ ), transpiration-based water-use efficiency (WUE;  $\text{gC m}^{-2} \text{mm}^{-1}$ ), mean vapour pressure deficit (VPD;  $\text{hPa}$ ), VPD seasonality ( $\text{VPD}_{\text{seas}}$ ;  $\text{hPa}$ ), and total  
 160 cloud cover (CLT; %). Except for RX5day, which is derived from daily precipitation, all variables are based on monthly mean output. The variable selection is based on the predictor screening described in Sect. 2.6. Seasonality, RX5day, VPD, and WUE are computed as follows.

Precipitation and VPD seasonality are defined as the standard deviation of the 12 monthly climatological means within each 30-year period. For a given variable  $X$  and monthly climatology  $\bar{X}_m$ , seasonality is computed as

$$X_{\text{seas}} = \sqrt{\frac{1}{12} \sum_{m=1}^{12} (\bar{X}_m - \bar{X})^2}, \quad (4)$$

165 where  $\bar{X}_m$  is the climatological mean for month  $m$  and  $\bar{X}$  is the mean of the 12 monthly climatological values.

RX5day is derived from daily precipitation as the annual maximum consecutive five-day precipitation. For a given year  $j$ ,

$$\text{RX5day}_j = \max(\text{RR}_{kj}), \quad (5)$$

where  $\text{RR}_{kj}$  denotes total precipitation accumulated over any five-day interval ending on day  $k$  within year  $j$ . For each 30-year period, RX5day is averaged over the annual maxima.

VPD is calculated using the Buck equation (Buck, 1981) to estimate saturation vapour pressure ( $e_s$ ),

$$e_s = 611.21 \times \exp \left[ \left( 18.678 - \frac{T}{234.5} \right) \left( \frac{T}{257.14 + T} \right) \right], \quad (6)$$

170 where  $T$  is near-surface air temperature in °C, and 611.21 Pa is the saturation vapour pressure at 0 °C. Actual vapour pressure ( $e_a$ ) is obtained from specific humidity ( $q$ ) and surface pressure ( $p_s$ , in Pa) as

$$e_a = \frac{qp_s}{0.622 + 0.378q}, \quad (7)$$

and VPD is then given by

$$\text{VPD} = e_s - e_a. \quad (8)$$

VPD is converted from Pa to hPa for the analysis.

We use the ratio of gross primary productivity (GPP) to transpiration to compute WUE, a widely used proxy for the CO<sub>2</sub> effect on stomatal resistance (Keenan et al., 2013; Lian et al., 2021; Ruehr et al., 2023):

$$\text{WUE} = \frac{\text{GPP}}{E_t}, \quad (9)$$

which quantifies the efficiency of carbon assimilation per unit of water consumed by vegetation through transpiration.

## 2.6 Multiple regression analysis

We construct multiple linear regression (MLR) models with Elastic Net regularisation separately for the two historical BGWS regimes to explain the spatial pattern of projected  $\Delta\text{BGWS}$  across grid cells. Each grid cell is treated as one sample, and both the predictors and the response variable are based on ensemble mean changes between the future and historical periods. The analysis therefore explains spatial differences in projected  $\Delta\text{BGWS}$  within each regime. It does not attribute the temporal evolution of BGWS at individual grid cells or regions.

Because neighbouring grid cells are not independent, we apply spatially blocked cross-validation. Grid cells are grouped into 10° × 20° latitude–longitude blocks, and all model training, tuning, and testing are performed using these spatial blocks as groups. For each regime, we apply repeated grouped train–test splits with 20% of the spatial blocks held out per repeat, combined with nested grouped cross-validation for Elastic Net hyperparameter tuning. To favour simpler models and reduce overfitting, the final hyperparameters are selected using a one-standard-error rule. Model performance is evaluated using out-of-sample  $R^2$  on held-out spatial blocks.

To address multicollinearity among predictors and to regularise the regression, we apply Elastic Net regularisation (Friedman et al., 2010). The Elastic Net objective function is

$$\min_{\beta} \left[ \frac{1}{2n} \sum_{i=1}^n (y_i - \hat{y}_i)^2 + \alpha \rho \sum_{j=1}^p |\beta_j| + \frac{\alpha(1-\rho)}{2} \sum_{j=1}^p \beta_j^2 \right], \quad (10)$$

where  $y_i$  and  $\hat{y}_i$  are the observed and predicted values,  $n$  is the number of samples,  $\beta_j$  are the regression coefficients,  $\alpha$  controls the overall regularisation strength, and  $\rho$  determines the balance between L1 (Lasso) and L2 (Ridge) penalties. The L1 penalty promotes sparsity by shrinking some coefficients to exactly zero, whereas the L2 penalty shrinks coefficients towards

zero without eliminating them, helping to stabilise estimates under multicollinearity. Prior to model fitting, all predictors are standardised to zero mean and unit variance within each training split, while  $\Delta\text{BGWS}$  is left on its original scale.

The final predictor set was selected from a larger initial set of candidate predictors according to their contribution to predictive performance, their physical interpretability, and data availability across the full 12-model ensemble (Sect. S2). The final set includes changes in mean precipitation, precipitation seasonality, RX5day, mean VPD, VPD seasonality, total cloud cover, near-surface soil moisture, LAI, and WUE. Together, these variables represent climatic and hydroecological processes relevant to climate change impacts and allow physical interpretation of their influence on  $\Delta\text{BGWS}$ . Changes in mean precipitation, precipitation seasonality, and extreme precipitation represent water supply and hydrological extremes. RX5day is used as the main extreme precipitation metric because multi-day precipitation accumulation shows slightly better spatial agreement than single-day extremes in CMIP6 and observational evaluations, making it a more robust indicator of extreme precipitation in large-scale datasets (Li et al., 2021a; Dunn et al., 2022). Changes in mean vapour pressure deficit and VPD seasonality represent atmospheric dryness and plant water stress. Changes in near-surface soil moisture represent surface water availability, while changes in LAI and WUE represent vegetation state and plant physiological responses to elevated  $\text{CO}_2$ . Changes in LAI reflect both climatic and human influences, including land-use and land-cover change, although these contributions are not isolated explicitly here. Changes in total cloud cover represent an additional atmospheric control related to energy and moisture conditions.

To quantify the contribution of each predictor to model performance, we compute permutation importance scores (Breiman, 2001). This model-agnostic metric is obtained by randomly permuting the values of a given predictor and quantifying the resulting change in  $R^2$ . For each repeat and each predictor, predictor values are permuted 20 times and the resulting decrease in  $R^2$  is recorded. We interpret these test-set importance scores as measures of the contribution of each predictor to the spatial pattern of projected  $\Delta\text{BGWS}$  within each regime. For comparison with the ensemble-mean attribution, we repeat the same blocked regression workflow for each individual ESM and report individual-model permutation importances only where mean held-out  $R^2 > 0.3$ .

### 3 Results and discussion

#### 3.1 Historical distribution of BGWS

The historical BGWS pattern in the CMIP6 ensemble mean (1985–2014; Fig. 1a) reveals three overarching features: energy-limited, water-limited, and precipitation-seasonality regulated blue–green water partitioning. The first two features are consistent with the broader literature distinguishing energy- and water-limited land-surface or ecosystem regimes, while the third extends this logic to precipitation-seasonality effects that are particularly relevant for blue–green water partitioning (Seneviratne et al., 2010; Denissen et al., 2022). On average, the area-weighted BGWS is slightly positive, indicating that  $\sim 2\%$  more precipitation is partitioned towards blue water flow, with notable ensemble variability from  $-16\%$  to  $+15\%$  (Table S4). These contrasts stem from differences in the model representation of precipitation characteristics, land-surface hydrology, and vegetation dynamics, which contribute to well-documented CMIP6 biases in simulated land-surface water fluxes relative to

reference products (Clark et al., 2015; Gentine et al., 2019; Zheng et al., 2019; Li et al., 2021b; Padrón et al., 2022; Yang et al., 2023).

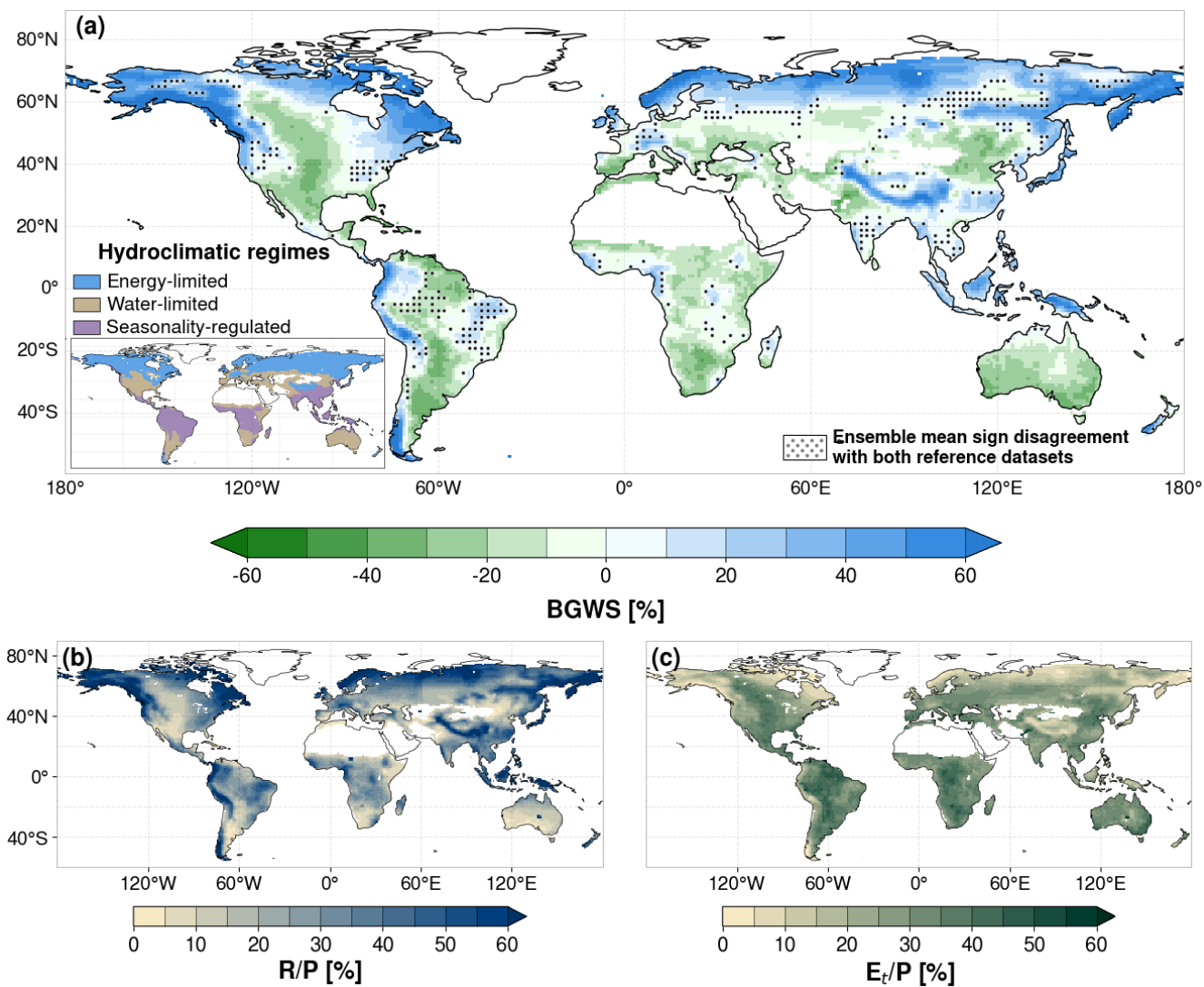


**Figure 1.** Ensemble mean for the historical period (1985–2014) based on 12 CMIP6 Earth system models. (a) BGWS [%] with inset showing a simple hydroclimatic regime classification in which each grid cell is assigned to the regime with the strongest standardized signal of low near-surface soil moisture, low air temperature, or high precipitation seasonality. (b) runoff share,  $R/P$  [%], and (c) transpiration share,  $E_t/P$  [%]. Blue colours in the BGWS colour map indicate a greater partitioning of precipitation towards runoff (blue water flow), whereas green colours indicate a greater partitioning towards transpiration (green water flow). Dots in panel (a) indicate regions where the sign of the ensemble mean BGWS disagrees with both reference datasets.

Comparing the spatial pattern of the ensemble mean BGWS with observation-based and reanalysis products indicates a reasonable large-scale representation for the historical climatology (Fig. S1). Agreement is weaker, but still qualitatively similar, for recent historical changes over the shorter evaluation period (Fig. S2). Compared with both reference datasets, the ensemble mean BGWS values are biased towards too much blue water. Decomposing BGWS into runoff ( $R/P$ ) and transpiration ( $E_t/P$ ) ratios shows that the bias is driven primarily by underestimated  $E_t/P$  (negative mean offset), while regional differences in  $R/P$  also contribute (Figs. S3 and S4). One possible structural contribution to the underestimated  $E_t/P$  bias is the limited representation of lateral groundwater redistribution in many large-scale land models used in ESMs, where this process is often overlooked or strongly simplified. By underrepresenting shallow groundwater support to ET in drylands or during dry periods, this may partly favour a more blue-biased BGWS (Maxwell and Condon, 2016; Liao et al., 2025). Accordingly, we treat BGWS as a process indicator and base interpretation primarily on directional patterns, sign-robust spatial structures, and covariation with relevant predictors, while avoiding detailed interpretation in regions with disagreement against both reference datasets (dots in Fig. 1a).

Energy-limited blue–green water partitioning, the first BGWS feature, is dominant across higher latitudes ( $> 60^\circ\text{N}$ ) and high-altitude regions, which consistently show greater partitioning towards blue water flow (Fig. 1a). This pattern aligns with the Budyko framework, which links energy-limited conditions to increased runoff (Budyko, 1974). In the higher latitudes, 95% of the land area exhibits a larger blue water share, with an area-weighted mean BGWS of +36 %. Here, low net radiation (light-limited) and low air temperatures (kinetic/phenology-limited) coincide with below-global-average  $E_t/P$ , while near-surface soil moisture remains comparatively high (Figs. 1c and S5). Consequently, precipitation predominantly contributes to runoff (Fig. 1b). Mountain ranges exhibit similar behaviour, where orographically enhanced precipitation and topography-controlled runoff parametrisations in ESMs (e.g., SIMTOP) can contribute to larger blue water shares (Niu et al., 2005; Gmann et al., 2025). Snowmelt-driven runoff likely further enhances blue water shares in cold regions (Barnett et al., 2005), although simplified representation of snow sublimation in ESMs may also contribute to runoff overestimation in some high-altitude regions and thus reinforce locally blue-biased partitioning (Stigter et al., 2018). Ongoing warming-related snow cover loss, by contrast, increases net radiation and ET and can reduce runoff (Milly and Dunne, 2020). Energy-limited partitioning is also evident across parts of the mid-latitudes ( $40\text{--}60^\circ\text{N/S}$ ), but with much smaller positive BGWS values than in the higher latitudes, with an area-weighted mean BGWS of about +4 %. This is consistent with seasonal transitions between winter energy limitation and summer water limitation (Seneviratne et al., 2010; Knoben et al., 2018). Compared with observation- and reanalysis-based products, however, the ensemble mean tends to overstate both the magnitude and the spatial extent of blue water shares in energy-limited high- and mid-latitudes (Fig. S1).

Water-limited blue–green water partitioning, the second BGWS feature, dominates in semi-arid and dry sub-humid regions such as the Eurasian Steppe or Australia’s Outback (Fig. 1a). These water-limited environments are marked by annual precipitation below the global mean and relatively low near-surface soil moisture (Fig. S5). Despite these hydrological constraints, these ecosystems partition a larger fraction of available water towards transpiration, increasing the green water share in line with observation-based data (Figs. 1 and S1). The RX5day-to-annual-precipitation ratio is elevated across many of these dryland regions (Fig. S6), indicating that rainfall is often temporally concentrated even where mean precipitation is low. Nevertheless,

within the retained vegetated drylands, the annual partitioning still tends to favour transpiration over runoff. This is consistent  
265 with water-limited ecosystems maintaining relatively low runoff fractions while using a large share of the limited incoming  
precipitation for vegetation water use (Althoff and Destouni, 2023).

Precipitation-seasonality regulated blue–green water partitioning, the third BGWS feature, emerges most clearly in mon-  
soonal and other strongly seasonal climates highlighted by the inset in Fig. 1a. In these regions, BGWS depends not only on  
how much precipitation falls annually, but also on how strongly rainfall is concentrated within the year. Regions with high  
270 precipitation seasonality, such as southern and eastern Asia and parts of the Maritime Continent, tend to show larger blue water  
shares where wet-season rainfall is strongly concentrated,  $RX5day$  is high, and near-surface soil moisture is comparatively  
high (Figs. 1 and S5). By contrast, humid regions with more weakly seasonal rainfall, such as much of the Amazon and central  
Africa, tend to show larger green water shares and higher  $E_t/P$ . Thus, the contrast is not simply between wet and dry regions,  
but between climates with strongly concentrated wet seasons and those with more even rainfall distribution. This mechanism  
275 is also consistent with the contrast between East Asian monsoon regions, which show larger blue water shares, and subtropical  
regions such as the Florida Peninsula, where more evenly distributed rainfall coincides with larger green water shares.

Overall, the historical BGWS distribution is therefore consistent with a transition from energy-limited blue-water dominance  
in cold and high-altitude regions, to water-limited green-water dominance in semi-arid regions, and to seasonality-regulated  
partitioning in monsoonal and humid subtropical climates. Several regions, especially within this third feature, also show  
280 disagreement with both reference datasets or elevated ensemble spread, underscoring the challenges ESMs still face in rep-  
resenting humid subtropical and tropical hydroecological dynamics (Fiedler et al., 2020; Padrón et al., 2022; Figs. 1a and  
S7).

### 3.2 Projected changes in BGWS

Figure 2a maps the projected BGWS changes (2071-2100 minus 1985-2014) under the regional rivalry scenario (SSP3-7.0),  
285 separated by whether grid cells historically belong to the blue or green water regime. The four change classes occupy broadly  
comparable fractions of the analysed land area. In the historical green water regime, 23% becomes greener and 33% less  
green; in the historical blue water regime, 20% becomes bluer and 24% less blue. Despite this broad balance in areal coverage,  
the ensemble-mean global BGWS increases slightly by +1.23 ppts (Table S4), with individual-model global mean changes  
ranging from  $-1.89$  to  $+4.99$  ppts. Regime shifts are less extensive than the strengthening or weakening of existing regimes,  
290 and occur more often from green to blue than from blue to green (Fig. S8). Because BGWS reflects the difference between  
runoff and transpiration relative to precipitation, a larger blue water share arises wherever runoff changes more positively than  
transpiration, whereas a larger green water share arises wherever transpiration changes more positively than runoff. The spatial  
expression of these mechanisms varies strongly across latitude bands and climate regimes (Fig. 2).

Larger blue water shares most directly occur where runoff increases more than transpiration increases. This pattern is evident  
295 in wetter parts of the historical blue water regime, for example, in northeastern Eurasia and along the East Asian monsoon belt,  
where enhanced precipitation coincides with increasing runoff and a strengthening of blue-water dominance (Fig. 2). In these  
regions, both blue and green water flows increase in absolute terms, but runoff gains are larger, so partitioning shifts further

towards blue water. Similar positive BGWS changes are also visible in historically blue-water dominated tropical regions such as large parts of India, where future trends are generally positive and coincide with increased wetting (Fig. 2).

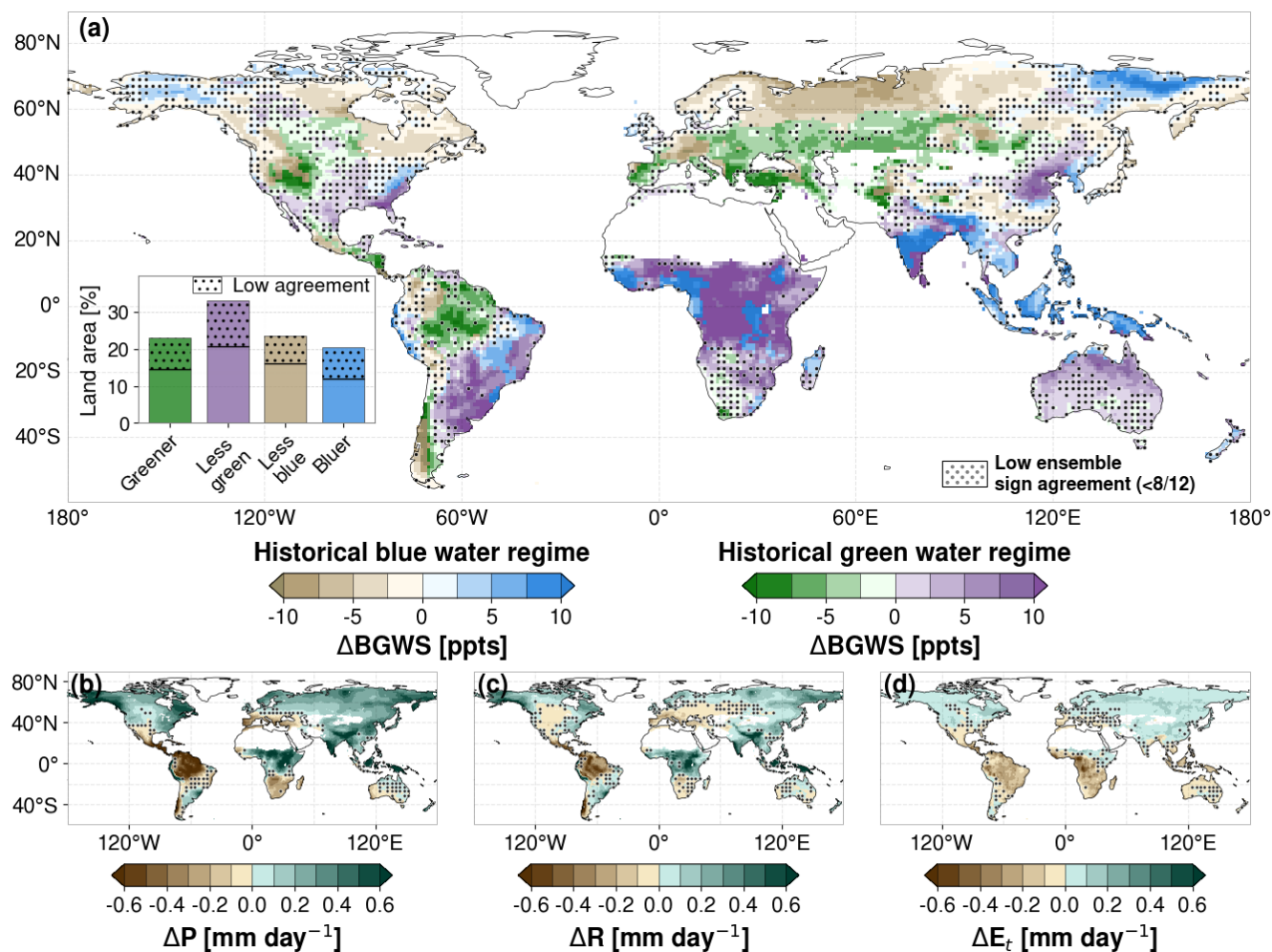


**Figure 2.** Ensemble mean change (2071–2100 minus 1985–2014) under the SSP3-7.0 scenario based on 12 CMIP6 Earth system models. (a)  $\Delta$ BGWS [ppts], shown separately for grid cells with historically positive BGWS values (blue water regime; beige to blue colours) and historically negative BGWS values (green water regime; green to purple colours). Blue and purple colours indicate shifts towards larger blue water shares, whereas green and beige colours indicate shifts towards larger green water shares. The inset summarises the analysed land-area fractions of the four BGWS-change classes; bar heights show the total area of each class, the horizontal line marks the fraction with robust sign agreement, and the stippled upper part indicates the fraction with low model agreement. (b)  $\Delta$  precipitation [ $\text{mm day}^{-1}$ ], (c)  $\Delta$  runoff [ $\text{mm day}^{-1}$ ], and (d)  $\Delta$  transpiration [ $\text{mm day}^{-1}$ ]. Stippling marks regions of low inter-model agreement, where fewer than 8 of the 12 models agree on the sign of change.

300 Larger blue water shares can also occur where runoff increases while transpiration decreases. This pattern is especially relevant in parts of the subtropics and tropics, where wetter conditions and increasing runoff coincide with declining transpiration. The major rainforests exhibit an asymmetric response in this respect: only the Amazon rainforest tends towards a greater green water share, whereas parts of central Africa and Maritime Southeast Asia shift towards greater blue water shares. This divergence coincides with precipitation and runoff increases in the latter two regions, while transpiration declines across all  
305 three rainforest regions (Fig. 2). Consistent with these regional examples, 68% of the analysed subtropical land and 77% of the analysed tropical land are projected to experience larger blue water shares.

A third pathway to larger blue water shares occurs where both runoff and transpiration decrease, but transpiration declines more strongly than runoff. This mechanism is visible in scattered historically water-limited patches of the subtropics and mid-latitudes, for example in parts of eastern Australia and northwestern Mexico (purple in Fig. 2a). In these regions, the  
310 relative decline in transpiration exceeds the runoff loss, shifting partitioning towards blue water even though absolute blue water flow may also decline. This contrasts with observed CO<sub>2</sub>-driven blue water losses where greening increased ET and reduced streamflow in Australia's sub-humid/semi-arid basins (Ukkola et al., 2016), and with vegetation-driven runoff declines in the American West (Mankin et al., 2017, 2019). While LAI increases across many of these regions, transpiration does not always rise in parallel because higher WUE can offset rising water demands (Figs. 2d and S9). More generally, whether  
315 dry regions will experience a blue or green water share increase depends largely on the interplay between rising vegetation water demand and WUE-related transpiration limitations, although structural uncertainties remain in how models represent vegetation responses to rising CO<sub>2</sub> and the resulting water-cycle impacts (Wei et al., 2024; Yang et al., 2021; Forzieri et al., 2020; Yang et al., 2023).

Larger green water shares occur where transpiration increases more than runoff increases. This mechanism is apparent in  
320 parts of the higher latitudes and mid-latitudes where leaf area expands and transpiration gains exceed the concurrent runoff increase, for example in northwestern Eurasia (Fig. S9). Consistent with this pattern, 62% of the analysed land area north of 60°N experiences a weakening of the historical blue water regime. Although a larger share of precipitation is partitioned towards green water flow, these regions concurrently experience an increase in blue water flow (Fig. 2c). In such cases, the shift towards green water does not necessarily imply a drying climate, but rather that transpiration becomes relatively more  
325 important than runoff.

A larger green water share can also arise where transpiration increases while runoff decreases. This pattern is particularly evident in parts of eastern Europe, where greener partitioning coincides with runoff loss (Fig. 2). In such cases, vegetation gains and enhanced transpiration shift the balance towards green water while blue water availability declines in absolute terms. The same logic applies to other mid-latitude regions where warming- and CO<sub>2</sub>-driven vegetation responses amplify transpiration  
330 despite weak or negative runoff trends.

Finally, larger green water shares occur where both runoff and transpiration decrease, but runoff declines more strongly than transpiration. This mechanism is evident in parts of southern Europe, where a greater reduction in runoff compared to transpiration results in a green water share increase (Fig. 2). This mechanism is also relevant in other regions with blue water losses, as receiving a smaller or only slightly larger share of precipitation does not offset the overall decline in runoff.

The regional BGWS changes described above suggest that future blue–green water partitioning reflects competing effects of changes in mean and extreme precipitation, changes in atmospheric and soil-moisture conditions, and vegetation responses. To quantify which selected predictors best explain the spatial pattern of  $\Delta$ BGWS within each historical regime, we fitted separate blocked multiple linear regression (MLR) models for the historical blue and green water regimes (Sect. 2.6). Figure 3 summarises the resulting permutation importance scores for the ensemble mean together with the corresponding importance ranks from individual ESMs. Both MLR models show moderate to strong predictive skill ( $R^2 = 0.49$  for the historical blue water regime and  $R^2 = 0.72$  for the historical green water regime). This interpretation and the importance rankings are further supported by the nonlinear Random Forest sensitivity analysis (Fig. S10).

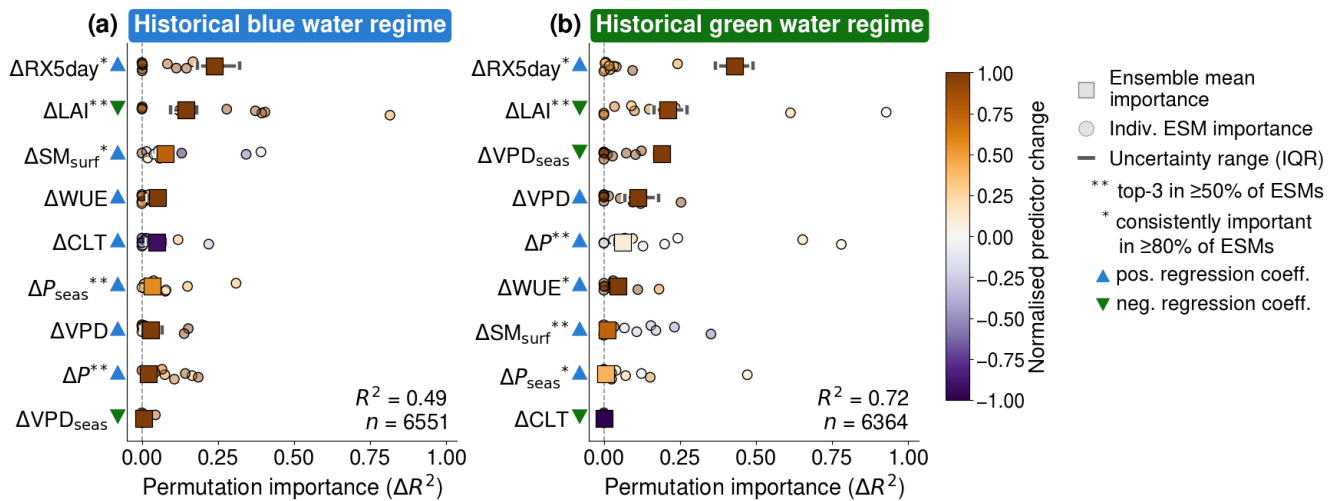


**Figure 3.** Variable importance for the spatial attribution of projected changes (2071–2100 minus 1985–2014) in  $\Delta$ BGWS under the SSP3-7.0 scenario in the two historical BGWS regimes shown in Fig. 2: (a) historical blue water regime and (b) historical green water regime. Squares show the median permutation importance ( $\Delta R^2$ ) of the 12-model CMIP6 ensemble mean for the predictor set, and horizontal lines show the interquartile range across repeated blocked cross-validation splits. Circles show the median permutation importance from individual ESMs with mean model performance  $R^2 > 0.3$ . Colours indicate the normalised mean change of each predictor within the respective regime. Upward blue triangles indicate positive regression coefficients and downward green triangles indicate negative regression coefficients in the ensemble mean. Reported  $R^2$  values give the mean model performance, and  $n$  is the number of grid cells in each regime.

Our results demonstrate that BGWS alterations in both regimes are most sensitive to extreme five-day precipitation changes (Fig. 3). RX5day is projected to increase across most of the global land area (Fig. S9), consistent with theoretical expectations that warming-driven increases in atmospheric moisture intensify precipitation extremes (Trenberth, 2011; Donat et al., 2016; Tabari, 2020). Its positive regression coefficient indicates that increases in RX5day are associated with larger blue water shares. This statistical relationship is physically plausible, because more intense multi-day rainfall can quickly saturate soils, triggering saturation-excess runoff in CMIP6 land-surface schemes. The RX5day effect would likely be even larger in models that also

350 represent infiltration-excess runoff, which only a few schemes currently include (Hou et al., 2023). Additionally, current coarse-resolution ESMS tend to underestimate precipitation extremes and often exhibit drizzle bias, suggesting that the hydrological influence of RX5day may be underestimated in our analysis (Brunner et al., 2025). The individual ESMS show that  $\Delta$ RX5day is an important predictor across most of the ensemble, but not consistently one of the top three predictors. This indicates that its dominance is strongest for the ensemble-mean BGWS field, whereas individual-model importance rankings are more variable.  
355 Such smoothing of model-specific noise and internal variability is a known consequence of multi-model averaging and helps isolate the common large-scale forced response, although it can also mask structural differences among models (Knutti et al., 2010).

Our findings emphasize two key points. First, even where mean precipitation decreases regionally, stronger increases in RX5day can still shift BGWS towards larger blue water shares. This suggests higher runoff sensitivity to intense rainfall  
360 even where average runoff is decreasing. Second, where mean precipitation also increases, larger RX5day changes can further enhance blue water shares because wetter mean conditions make saturation-driven runoff during extreme precipitation events more likely. This helps explain why  $\Delta$ RX5day emerges as the dominant positive predictor of  $\Delta$ BGWS despite contrasting regional trends in mean precipitation.

The dominant role of  $\Delta$ RX5day is consistent with studies showing strong effects of rainfall extremes on runoff ratios and  
365 catchment retention (Yang et al., 2018; Scheff et al., 2022). We extend this insight from retention and runoff-based metrics to a partitioning metric that also includes transpiration, linking precipitation intensity and plant water use to the balance between runoff and transpiration. Whereas Mankin et al. (2018) found that runoff partitioning changes are governed by precipitation changes, including mean precipitation and five-day precipitation extremes, our results identify extreme five-day precipitation as the leading spatial predictor of projected BGWS change.

370 The strongest negative predictor of the ensemble mean  $\Delta$ BGWS field in both regimes is  $\Delta$ LAI, which is strongly supported by the individual ESM results (Fig. 3). Larger increases in LAI are associated with greener partitioning, indicating that vegetation expansion tends to favour transpiration relative to runoff. This provides the main counterweight to the positive RX5day effect and helps explain why blue-to-green shifts still occupy a substantial fraction of global land area despite the dominant blueward influence of extreme precipitation. Global greening is evident in the ensemble mean, with larger LAI increases in the  
375 historical blue water regime (Fig. S9). Particularly blue water-dominated higher and mid-latitudes experience extensive vegetation growth due to global warming, where energy and temperature limitation is the primary controlling factor. In addition, CO<sub>2</sub> fertilisation and scenario-dependent land-use changes further impact LAI (Hurt et al., 2020; Zhao et al., 2020). Overall, larger LAI is associated with increased transpiration water demand and may also increase canopy interception losses, thereby reducing throughfall and runoff and potentially reinforcing green-ward shifts.

380 Beyond the two dominant predictors, the importance structure differs between the two historical regimes. In the blue water regime,  $\Delta$ SM<sub>surf</sub> is the third most important predictor in the ensemble mean, indicating that wetter near-surface soils favour larger blue water shares. This is consistent with the blue water regime being concentrated in already wet, energy-limited, or seasonally wet regions, where further increases in near-surface soil moisture help maintain or strengthen runoff-dominated partitioning by increasing the likelihood of saturation-driven runoff (Singh et al., 2021). In the green water regime,  $\Delta$ VPD<sub>seas</sub>

385 is the third most important predictor in the ensemble mean, suggesting that stronger seasonal atmospheric dryness favours  
greener partitioning. This is consistent with the green water regime being concentrated in water-limited or strongly seasonal  
climates, where the seasonal contrast in atmospheric moisture demand remains an important control on transpiration-dominated  
partitioning (Seneviratne et al., 2010; Young et al., 2022). The exact ranking of lower-order predictors, however, is less stable  
and should not be overemphasised, because differences in ensemble-mean permutation importance are small and rankings also  
390 vary across individual ESMs. In summary, the predictor rankings suggest that projected BGWS changes arise primarily from  
the interplay between precipitation intensification and vegetation expansion, while plant-atmosphere controls on transpiration  
and changes in near-surface wetness emerge as additional regionally relevant predictors.

### 3.4 Implications of future BGWS trends

The BGWS metric is a process rather than a quantity indicator. It characterises how an incremental unit of precipitation (e.g.,  
395 the next millimetre of rain) is partitioned between runoff (blue water) and plant use via transpiration (green water), not how  
large those fluxes are in absolute terms. In this sense, BGWS addresses the question "where does the next unit of rain tend to  
go?" rather than "how much water is there overall?". As our analysis excludes hyper-arid and sparsely vegetated regions, this  
distinction matters for impacts that depend on hydrological sensitivity and timing (Nijssen et al., 2001). It shifts the focus from  
one on absolute change, to one in which we try to understand controlling factors and enables another level of model evaluation  
400 that centres on comparing these controlling factors rather than just focusing on matching historical observations (Wagener  
et al., 2022). Although our analysis is flow-based and excludes storage terms, persistent BGWS shifts signal sustained pressure  
on blue water stores (e.g., rivers, reservoirs, groundwater) versus green water stores (root-zone moisture).

BGWS changes become most meaningful when interpreted jointly with absolute changes in runoff and transpiration rather  
than in isolation (Fig. 4). In combination with runoff changes (Fig. 4a), the robust sign combinations point to four distinct  
405 hydrological implications. Where  $\Delta\text{BGWS}$  and  $\Delta R$  are both positive, both runoff volume and the runoff share of precipitation  
increase, indicating stronger blue-water partitioning and greater potential for high-flow pressure during wet periods (e.g.,  
southern Asia); where  $\Delta\text{BGWS}$  is positive but  $\Delta R$  is negative, runoff shrinks in absolute terms but its share of precipitation  
still increases. Thus, the relative contribution of runoff pathways per unit precipitation increases, indicating higher runoff  
sensitivity to intense rainfall. Yet, this pattern occurs only rarely in the robust map. Conversely, negative  $\Delta\text{BGWS}$  with positive  
410  $\Delta R$  suggests more total runoff but a smaller share of precipitation, implying that runoff may remain elevated if water supply  
stays sufficient (e.g., northwestern Eurasia); where both  $\Delta\text{BGWS}$  and  $\Delta R$  are negative, shrinking blue water volumes and  
shares indicate concurrent pressure on blue-water supply (e.g., large parts of Europe). Comparable patterns are seen during  
European droughts, where blue water declines outpace green water responses, tightening low-flows even when vegetation  
maintains transpiration (Orth and Destouni, 2018).

415 Joint interpretation of BGWS with transpiration changes adds eco-physiological and land-surface insight (Fig. 4b). Where  
 $\Delta\text{BGWS}$  and  $\Delta E_t$  are both positive, landscapes become more runoff-dominated while plant water use rises, consistent with  
higher atmospheric/phenological demand and greater reliance on stored water (e.g., northeastern Eurasia); where  $\Delta\text{BGWS}$  is  
positive and  $\Delta E_t$  is negative, partitioning shifts toward runoff as vegetation down-regulates (e.g., southeastern South America).

The latter response reduces evaporative cooling and elevates heat risk (He et al., 2022). Conversely, where  $\Delta BGWS$  is negative and  $\Delta E_t$  is positive, regions experience greener partitioning, which may strengthen land–atmosphere coupling and support stronger latent cooling (e.g., northeastern North America); when both  $\Delta BGWS$  and  $\Delta E_t$  decrease, relative allocation to green water rises despite lower plant water use, which points to weaker evaporative cooling and vegetation-mediated buffering of heat and moisture stress (e.g., parts of the Amazon rainforest).

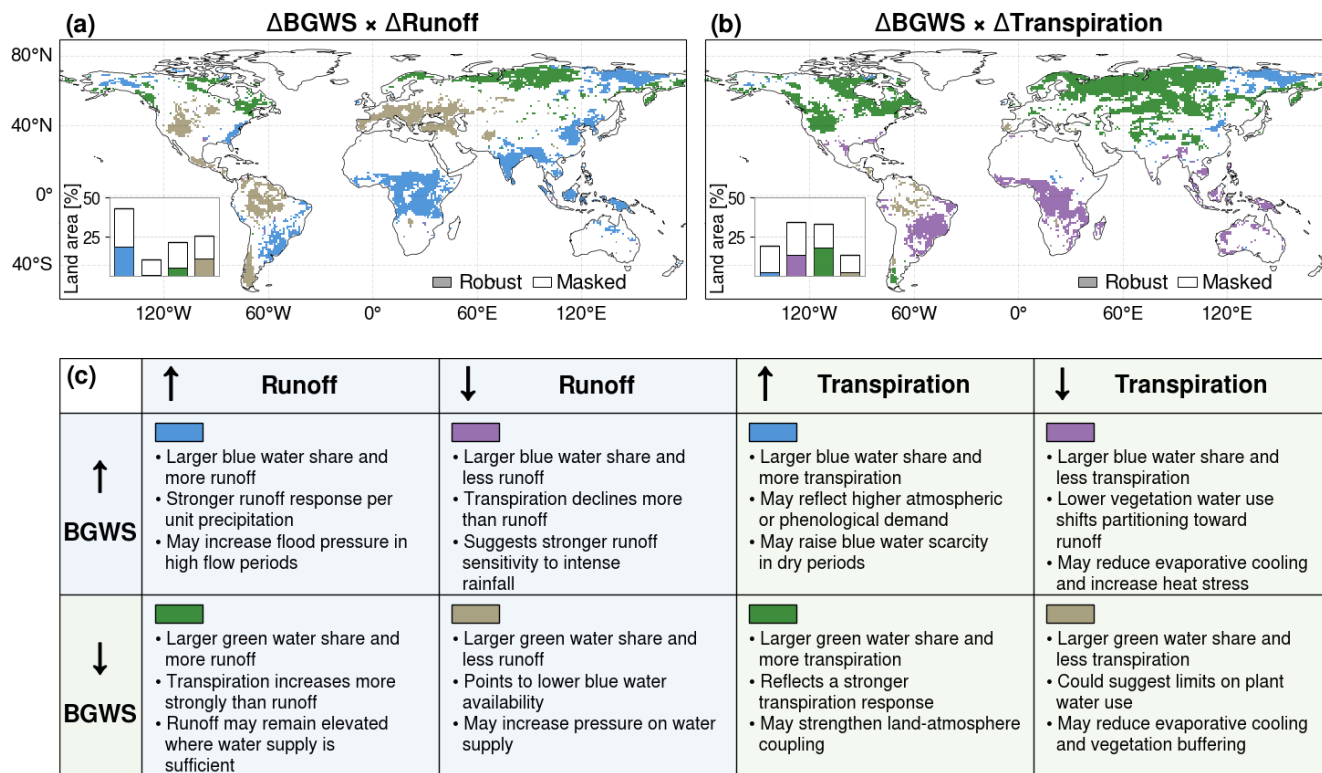


**Figure 4.** Projected changes in blue–green water partitioning and associated runoff and transpiration responses. Panels (a) and (b) show the ensemble mean  $\Delta BGWS$  combined with changes in runoff and transpiration, respectively, for the end of the century relative to the historical period. Colours indicate the four joint sign combinations between  $\Delta BGWS$  and the corresponding flux change, as defined schematically in panel (c), which also summarises their possible hydroecological implications. White grid cells in panels (a) and (b) denote areas excluded by the historical analysis mask or masked because fewer than 8 of the 12 models agree on the same joint quadrant class. Insets show the land-area fraction of each quadrant class, with coloured bar segments indicating robust area and white segments indicating area masked because of low agreement.

In communicating results, it is important to make uncertainty explicit. Fig. 4 therefore only shows areas where at least eight of the twelve models agree on the sign of both  $\Delta BGWS$  and the corresponding flux change. Even so, the results should be read as robust regional tendencies rather than local predictions. In regions with robust sign agreement, joint interpretation of  $\Delta BGWS$  with  $\Delta R$  and  $\Delta E_t$  provides a compact way to distinguish whether future change is more likely to intensify runoff

sensitivity, strengthen transpiration demand, or simultaneously reduce water availability and vegetation cooling. Given the additional baseline biases relative to reanalysis and observation-based products (Sect. S3), a regionalised and observationally constrained analysis of  $\Delta$ BGWS and co-varying hydroecological responses would still be needed before drawing site-specific management conclusions.

#### 4 Conclusions

In this study, we assessed where future blue–green water partitioning shifts favour blue or green water pathways and which climatic and hydroecological changes are associated with these shifts. To do so, we defined the BGWS and applied it to 12 CMIP6 ESMs under SSP3–7.0, focusing on vegetated and hydrologically active land areas. Together, the results show distinct historical partitioning regimes, spatially heterogeneous future shifts, and a dominant role of precipitation intensification that is partly counteracted by vegetation expansion.

Historically, BGWS separates cold, high-altitude, and strongly seasonal regions with larger blue water shares from many water-limited regions with larger green water shares. Future changes show a slight ensemble-mean shift towards larger blue water shares, with strengthening or weakening of existing regimes more common than full regime shifts. The main predictor of projected BGWS change is increasing extreme five-day precipitation, which favours larger blue water shares, while increasing LAI provides the main counterweight by favouring vegetation-mediated green water use. Interpreting BGWS together with absolute runoff and transpiration changes helps distinguish where future changes may increase runoff sensitivity, strengthen vegetation water use, reduce blue water availability, or weaken vegetation-mediated cooling.

Nonetheless, uncertainties and biases in ESM studies remain because BGWS dynamics depend on the representation of hydroclimatic and biogeochemical processes (Clark et al., 2015; Gentine et al., 2019; Zheng et al., 2019; Padrón et al., 2022; Yang et al., 2023; Gier et al., 2024). An additional source of uncertainty is that many large-scale land models used in ESMs still represent lateral groundwater redistribution only in a limited or highly simplified way, partly because coarse model resolution does not resolve subgrid land-surface heterogeneity well (Liao et al., 2025). This can affect blue–green water partitioning by underrepresenting shallow groundwater support to ET during dry periods, potentially favouring a more blue-biased partitioning (Maxwell and Condon, 2016).

Despite these uncertainties, particularly in the land-surface components and their assumptions regarding plant responses to elevated CO<sub>2</sub>, robust signals of BGWS shifts within the ESM ensemble emerge. While we used LAI as a proxy for vegetation responses that reflect both climatic and human influences, future research could assess land-use and land-cover changes more explicitly. Additionally, advancing both observational data and ESMs appears vital to improve the reliability of future projections on terrestrial freshwater availability, including a more consistent treatment of human influences such as irrigation. Coupling these advances with process-based ESM evaluations can deepen insights into blue–green water partitioning and vegetation–climate feedbacks and support more robust climate information, especially in understudied, high-impact regions (Stein et al., 2024).

460 *Code and data availability.* The CMIP6 datasets used in this study were accessed through the Deutsche Klimarechenzentrum (DKRZ) CMIP Data Pool (last access: 20 June 2025) and the Earth System Grid Federation (<https://aims2.llnl.gov>) portal. The DKRZ CMIP Data Pool (available at <https://cmip-data-pool.dkrz.de>) is restricted to registered users with a valid DKRZ account. The GPCC monthly product is available for download from DWD Open Data: [https://opendata.dwd.de/climate\\_environment/GPCC/html/fulldata-monthly\\_v2022\\_doi\\_download.html](https://opendata.dwd.de/climate_environment/GPCC/html/fulldata-monthly_v2022_doi_download.html) (last access: 10 January 2025). The G-RUN dataset is publicly available at Figshare: [https://figshare.com/articles/dataset/G-RUN\\_ENSEMBLE/12794075](https://figshare.com/articles/dataset/G-RUN_ENSEMBLE/12794075) (last access: 10 January 2025). The GLEAM dataset is available via SFTP (Secure File Transfer Protocol) and requires user registration for access. Credentials can be requested at GLEAM website: <https://www.gleam.eu> (last access: 10 January 2025). ERA5-Land data is publicly available through the Copernicus CDS (last access: 10 January 2025). All code to reproduce this analysis is publicly available on GitHub at: [https://github.com/simonheselschwerdt/bgws\\_analysis](https://github.com/simonheselschwerdt/bgws_analysis).

470 *Author contributions.* S.P.H. and P.G. conceived the study and designed the analysis. S.P.H. conducted the analysis and led the writing of the manuscript. All authors discussed the methods and results and contributed to writing and edited the manuscript.

*Competing interests.* Some authors are members of the editorial board of Earth System Dynamics.

475 *Acknowledgements.* This study is financially supported by the Helmholtz Association Initiative and Networking Fund (IVF). We acknowledge the World Climate Research Programme's Working Group on Coupled Modelling, which is responsible for CMIP, and we thank the climate modelling groups for producing and making available their model output. This work used resources of the Deutsches Klimarechenzentrum (DKRZ, <https://www.dkrz.de>) granted by its Scientific Steering Committee (WLA) under project ID ch0636. S.P.H. and P.G. also thank Peter Hoffmann for internally reviewing our paper draft. T.W. acknowledges support from the Alexander von Humboldt Foundation in the framework of the Alexander von Humboldt Professorship endowed by the German Federal Ministry of Education and Research (BMBF). L.W.-E. acknowledges financial support from Formas - a Swedish Research Council for Sustainable Development (2022-02089, 2023-00310, 2023-00321).

## 480 References

- Althoff, D. and Destouni, G.: Global patterns in water flux partitioning: Irrigated and rainfed agriculture drives asymmetrical flux to vegetation over runoff, *One Earth*, 6, 1246–1257, <https://doi.org/10.1016/j.oneear.2023.08.002>, 2023.
- Barnett, T. P., Adam, J. C., and Lettenmaier, D. P.: Potential impacts of a warming climate on water availability in snow-dominated regions, *Nature*, 438, 303–309, <https://doi.org/10.1038/nature04141>, 2005.
- 485 Berg, A. and Sheffield, J.: Evapotranspiration Partitioning in CMIP5 Models: Uncertainties and Future Projections, *Journal of Climate*, 32, 2653–2671, <https://doi.org/10.1175/JCLI-D-18-0583.1>, 2019.
- Bouaziz, L. J. E., Aalbers, E. E., Weerts, A. H., Hegnauer, M., Buiteveld, H., Lammersen, R., Stam, J., Sprokkereef, E., Savenije, H. H. G., and Hrachowitz, M.: Ecosystem adaptation to climate change: the sensitivity of hydrological predictions to time-dynamic model parameters, *Hydrology and Earth System Sciences*, 26, 1295–1318, <https://doi.org/10.5194/hess-26-1295-2022>, 2022.
- 490 Boucher, O., Servonnat, J., Albright, A. L., Aumont, O., Balkanski, Y., Bastrikov, V., Bekki, S., Bonnet, R., Bony, S., Bopp, L., Braconnot, P., Brockmann, P., Cadule, P., Caubel, A., Cheruy, F., Codron, F., Cozic, A., Cugnet, D., D’Andrea, F., Davini, P., de Lavergne, C., Denvil, S., Deshayes, J., Devilliers, M., Ducharne, A., Dufresne, J.-L., Dupont, E., Éthé, C., Fairhead, L., Falletti, L., Flavoni, S., Foujols, M.-A., Gardoll, S., Gastineau, G., Ghattas, J., Grandpeix, J.-Y., Guenet, B., Guez, Lionel, E., Guilyardi, E., Guimberteau, M., Hauglustaine, D., Hourdin, F., Idelkadi, A., Joussaume, S., Kageyama, M., Khodri, M., Krinner, G., Lebas, N., Levvasseur, G., Lévy, C., Li, L., Lott, F.,
- 495 Lurton, T., Luysaert, S., Madec, G., Madeleine, J.-B., Maignan, F., Marchand, M., Marti, O., Mellul, L., Meurdesoif, Y., Mignot, J., Musat, I., Otlé, C., Peylin, P., Planton, Y., Polcher, J., Rio, C., Rochetin, N., Rousset, C., Sepulchre, P., Sima, A., Swingedouw, D., Thiéblemont, R., Traore, A. K., Vancoppenolle, M., Vial, J., Vialard, J., Viovy, N., and Vuichard, N.: Presentation and Evaluation of the IPSL-CM6A-LR Climate Model, *Journal of Advances in Modeling Earth Systems*, 12, e2019MS002 010, <https://doi.org/10.1029/2019MS002010>, 2020.
- Breiman, L.: Random Forests, *Machine Learning*, 45, 5–32, <https://doi.org/10.1023/A:1010933404324>, 2001.
- 500 Brunner, L., Poschlod, B., Dutra, E., Fischer, E. M., Martius, O., and Sillmann, J.: A global perspective on the spatial representation of climate extremes from km-scale models, *Environmental Research Letters*, 20, 074 054, <https://doi.org/10.1088/1748-9326/ade1ef>, 2025.
- Buck, A. L.: New Equations for Computing Vapor Pressure and Enhancement Factor, *Journal of Applied Meteorology and Climatology*, 20, 1527–1532, [https://doi.org/10.1175/1520-0450\(1981\)020<1527:NEFCVP>2.0.CO;2](https://doi.org/10.1175/1520-0450(1981)020<1527:NEFCVP>2.0.CO;2), 1981.
- Budyko, M. I.: *Climate and Life*, Academic Press, New York, 1974.
- 505 Clark, M. P., Fan, Y., Lawrence, D. M., Adam, J. C., Bolster, D., Gochis, D. J., Hooper, R. P., Kumar, M., Leung, L. R., Mackay, D. S., Maxwell, R. M., Shen, C., Swenson, S. C., and Zeng, X.: Improving the representation of hydrologic processes in Earth System Models, *Water Resources Research*, 51, 5929–5956, <https://doi.org/10.1002/2015WR017096>, 2015.
- Danabasoglu, G., Lamarque, J.-F., Bacmeister, J., Bailey, D. A., DuVivier, A. K., Edwards, J., Emmons, L. K., Fasullo, J., Garcia, R., Gettelman, A., Hannay, C., Holland, M. M., Large, W. G., Lauritzen, P. H., Lawrence, D. M., Lenaerts, J. T. M., Lindsay, K., Lipscomb,
- 510 W. H., Mills, M. J., Neale, R., Oleson, K. W., Otto-Bliesner, B., Phillips, A. S., Sacks, W., Tilmes, S., van Kampenhout, L., Vertenstein, M., Bertini, A., Dennis, J., Deser, C., Fischer, C., Fox-Kemper, B., Kay, J. E., Kinnison, D., Kushner, P. J., Larson, V. E., Long, M. C., Mickelson, S., Moore, J. K., Nienhouse, E., Polvani, L., Rasch, P. J., and Strand, W. G.: The Community Earth System Model Version 2 (CESM2), *Journal of Advances in Modeling Earth Systems*, 12, e2019MS001 916, <https://doi.org/10.1029/2019MS001916>, 2020.
- Denissen, J. M. C., Teuling, A. J., Pitman, A. J., Koirala, S., Migliavacca, M., Li, W., Reichstein, M., Winkler, A. J., Zhan, C., and Orth,
- 515 R.: Widespread shift from ecosystem energy to water limitation with climate change, *Nature Climate Change*, 12, 677–684, <https://www.nature.com/articles/s41558-022-01403-8>, 2022.

- Donat, M. G., Lowry, A. L., Alexander, L. V., O’Gorman, P. A., and Maher, N.: More extreme precipitation in the world’s dry and wet regions, *Nature Climate Change*, 6, 508–513, <https://doi.org/10.1038/nclimate2941>, 2016.
- 520 Dunn, R. J. H., Donat, M. G., and Alexander, L. V.: Comparing extremes indices in recent observational and reanalysis products, *Frontiers in Climate*, 4, <https://doi.org/10.3389/fclim.2022.989505>, 2022.
- Dunne, J. P., Horowitz, L. W., Adcroft, A. J., Ginoux, P., Held, I. M., John, J. G., Krasting, J. P., Malyshev, S., Naik, V., Paulot, F., Shevliakova, E., Stock, C. A., Zadeh, N., Balaji, V., Blanton, C., Dunne, K. A., Dupuis, C., Durachta, J., Dussin, R., Gauthier, P. P. G., Griffies, S. M., Guo, H., Hallberg, R. W., Harrison, M., He, J., Hurlin, W., McHugh, C., Menzel, R., Milly, P. C. D., Nikonov, S., Paynter, D. J., Ploshay, J., Radhakrishnan, A., Rand, K., Reichl, B. G., Robinson, T., Schwarzkopf, D. M., Sentman, L. T., Underwood, S., Vahlenkamp, H., Winton, 525 M., Wittenberg, A. T., Wyman, B., Zeng, Y., and Zhao, M.: The GFDL Earth System Model Version 4.1 (GFDL-ESM 4.1): Overall Coupled Model Description and Simulation Characteristics, *Journal of Advances in Modeling Earth Systems*, 12, e2019MS002015, <https://doi.org/10.1029/2019MS002015>, eprint: <https://onlinelibrary.wiley.com/doi/pdf/10.1029/2019MS002015>, 2020.
- Dutta, R. and Markonis, Y.: Does ERA5-land capture the changes in the terrestrial hydrological cycle across the globe?, *Environmental Research Letters*, 19, 024054, <https://doi.org/10.1088/1748-9326/ad1d3a>, 2024.
- 530 Döscher, R., Acosta, M., Alessandri, A., Anthoni, P., Arsouze, T., Bergman, T., Bernardello, R., Boussetta, S., Caron, L.-P., Carver, G., Castrillo, M., Catalano, F., Cvijanovic, I., Davini, P., Dekker, E., Doblas-Reyes, F. J., Docquier, D., Echevarria, P., Fladrich, U., Fuentes-Franco, R., Gröger, M., v. Hardenberg, J., Hieronymus, J., Karami, M. P., Keskinen, J.-P., Koenigk, T., Makkonen, R., Massonnet, F., Ménégos, M., Miller, P. A., Moreno-Chamarro, E., Nieradzick, L., van Noije, T., Nolan, P., O’Donnell, D., Ollinaho, P., van den Oord, G., Ortega, P., Prims, O. T., Ramos, A., Reerink, T., Rousset, C., Ruprich-Robert, Y., Le Sager, P., Schmith, T., Schrödner, R., Serva, F., 535 Sicardi, V., Sloth Madsen, M., Smith, B., Tian, T., Tourigny, E., Uotila, P., Vancoppenolle, M., Wang, S., Wärlind, D., Willén, U., Wyser, K., Yang, S., Yepes-Arbós, X., and Zhang, Q.: The EC-Earth3 Earth system model for the Coupled Model Intercomparison Project 6, *Geoscientific Model Development*, 15, 2973–3020, <https://doi.org/10.5194/gmd-15-2973-2022>, 2022.
- Eekhout, J. P. C., Hunink, J. E., Terink, W., and de Vente, J.: Why increased extreme precipitation under climate change negatively affects water security, *Hydrology and Earth System Sciences*, 22, 5935–5946, <https://doi.org/10.5194/hess-22-5935-2018>, 2018.
- 540 Eyring, V., Bony, S., Meehl, G. A., Senior, C. A., Stevens, B., Stouffer, R. J., and Taylor, K. E.: Overview of the Coupled Model Intercomparison Project Phase 6 (CMIP6) experimental design and organization, *Geoscientific Model Development*, 9, 1937–1958, <https://doi.org/10.5194/gmd-9-1937-2016>, 2016.
- Falkenmark, M.: Land–water linkages: a synopsis, in: *Land and Water Integration and River Basin Management*, Proceedings of the FAO Workshop, Rome, 31 January–2 February 1993, pp. 15–17, FAO, Rome, <https://www.fao.org/4/v5400e/v5400e00.htm>, 1995.
- 545 Falkenmark, M.: Growing water scarcity in agriculture: future challenge to global water security, *Philosophical Transactions of the Royal Society A: Mathematical, Physical and Engineering Sciences*, 371, 20120410, <https://doi.org/10.1098/rsta.2012.0410>, 2013.
- Falkenmark, M. and Rockström, J.: The New Blue and Green Water Paradigm: Breaking New Ground for Water Resources Planning and Management, *Journal of Water Resources Planning and Management*, 132, 129–132, [https://doi.org/10.1061/\(ASCE\)0733-9496\(2006\)132:3\(129\)](https://doi.org/10.1061/(ASCE)0733-9496(2006)132:3(129)), 2006.
- 550 Falkenmark, M., Wang-Erlandsson, L., and Rockström, J.: Understanding of water resilience in the Anthropocene, *Journal of Hydrology X*, 2, 100009, <https://doi.org/10.1016/j.hydroa.2018.100009>, 2019.
- Fiedler, S., Crueger, T., D’Agostino, R., Peters, K., Becker, T., Leutwyler, D., Paccini, L., Burdanowitz, J., Buehler, S. A., Cortes, A. U., Dauhut, T., Dommenges, D., Fraedrich, K., Jungandreas, L., Maher, N., Naumann, A. K., Rugenstein, M., Sakradzija, M., Schmidt, H., Sielmann, F., Stephan, C., Timmreck, C., Zhu, X., and Stevens, B.: Simulated Tropical Precipitation Assessed across Three Ma-

- 555 jor Phases of the Coupled Model Intercomparison Project (CMIP), *Monthly Weather Review*, 148, 3653–3680, <https://doi.org/10.1175/MWR-D-19-0404.1>, 2020.
- Forzieri, G., Miralles, D. G., Ciais, P., Alkama, R., Ryu, Y., Duveiller, G., Zhang, K., Robertson, E., Kautz, M., Martens, B., Jiang, C., Armeth, A., Georgievski, G., Li, W., Ceccherini, G., Anthoni, P., Lawrence, P., Wiltshire, A., Pongratz, J., Piao, S., Sitch, S., Goll, D. S., Arora, V. K., Lienert, S., Lombardozi, D., Kato, E., Nabel, J. E. M. S., Tian, H., Friedlingstein, P., and Cescatti, A.: Increased control of  
560 vegetation on global terrestrial energy fluxes, *Nature Climate Change*, 10, 356–362, <https://doi.org/10.1038/s41558-020-0717-0>, 2020.
- Friedman, J. H., Hastie, T., and Tibshirani, R.: Regularization Paths for Generalized Linear Models via Coordinate Descent, *Journal of Statistical Software*, 33, 1–22, <https://doi.org/10.18637/jss.v033.i01>, 2010.
- Fujimori, S., Hasegawa, T., Masui, T., Takahashi, K., Herran, D. S., Dai, H., Hijioka, Y., and Kainuma, M.: SSP3: AIM implementation of Shared Socioeconomic Pathways, *Global Environmental Change*, 42, 268–283, <https://doi.org/10.1016/j.gloenvcha.2016.06.009>, 2017.
- 565 Gentine, P., Green, J. K., Guérin, M., Humphrey, V., Seneviratne, S. I., Zhang, Y., and Zhou, S.: Coupling between the terrestrial carbon and water cycles—a review, *Environmental Research Letters*, 14, 083 003, <https://doi.org/10.1088/1748-9326/ab22d6>, 2019.
- Ghiggi, G., Humphrey, V., Seneviratne, S. I., and Gudmundsson, L.: GRUN: an observation-based global gridded runoff dataset from 1902 to 2014, *Earth System Science Data*, 11, 1655–1674, <https://doi.org/10.5194/essd-11-1655-2019>, 2019.
- Gier, B. K., Schlund, M., Friedlingstein, P., Jones, C. D., Jones, C., Zaehle, S., and Eyring, V.: Representation of the terrestrial carbon cycle  
570 in CMIP6, *Biogeosciences*, 21, 5321–5360, <https://doi.org/10.5194/bg-21-5321-2024>, 2024.
- Gleeson, T., Wang-Erlandsson, L., Porkka, M., Zipper, S. C., Jaramillo, F., Gerten, D., Fetzer, I., Cornell, S. E., Piemontese, L., Gordon, L. J., Rockström, J., Oki, T., Sivapalan, M., Wada, Y., Brauman, K. A., Flörke, M., Bierkens, M. F. P., Lehner, B., Keys, P., Kummu, M., Wagener, T., Dadson, S., Troy, T. J., Steffen, W., Falkenmark, M., and Famiglietti, J. S.: Illuminating water cycle modifications and Earth system resilience in the Anthropocene, *Water Resources Research*, 56, e2019WR024 957, <https://doi.org/10.1029/2019WR024957>, 2020.
- 575 Gnann, S., Baldwin, J. W., Cuthbert, M. O., Gleeson, T., Schwanghart, W., and Wagener, T.: The Influence of Topography on the Global Terrestrial Water Cycle, *Reviews of Geophysics*, 63, e2023RG000 810, <https://doi.org/10.1029/2023RG000810>, 2025.
- Greve, P., Orłowsky, B., Mueller, B., Sheffield, J., Reichstein, M., and Seneviratne, S. I.: Global assessment of trends in wetting and drying over land, *Nature Geoscience*, 7, 716–721, <https://doi.org/10.1038/ngeo2247>, 2014.
- Gudmundsson, L., Brunner, M. I., Döll, P., Fluet-Chouinard, E., Frolova, N., Gosling, S. N., Hirabayashi, Y., Kireeva, M. B., Liu, X.,  
580 Müller Schmied, H., Magritskiy, D., Slater, L. J., Stein, L., Trambly, Y., Wang, K., Wasko, C., Yamazaki, D., and Zhou, X.: Past and future change in global river flows, *Nature Reviews Earth & Environment*, 7, 7–23, <https://doi.org/10.1038/s43017-025-00745-z>, 2026.
- Hajima, T., Watanabe, M., Yamamoto, A., Tatebe, H., Noguchi, M. A., Abe, M., Ohgaito, R., Ito, A., Yamazaki, D., Okajima, H., Ito, A., Takata, K., Ogochi, K., Watanabe, S., and Kawamiya, M.: Development of the MIROC-ES2L Earth system model and the evaluation of biogeochemical processes and feedbacks, *Geoscientific Model Development*, 13, 2197–2244, <https://doi.org/10.5194/gmd-13-2197-2020>,  
585 2020.
- Han, J., Yang, Y., Roderick, M. L., McVicar, T. R., Yang, D., Zhang, S., and Beck, H. E.: Assessing the Steady-State Assumption in Water Balance Calculation Across Global Catchments, *Water Resources Research*, 56, e2020WR027 392, <https://doi.org/10.1029/2020WR027392>, 2020.
- Hausfather, Z. and Peters, G. P.: Emissions – the ‘business as usual’ story is misleading, *Nature*, 577, 618–620, <https://doi.org/10.1038/d41586-020-00177-3>, 2020.  
590

- He, M., Piao, S., Huntingford, C., Xu, H., Wang, X., Bastos, A., Cui, J., and Gasser, T.: Amplified warming from physiological responses to carbon dioxide reduces the potential of vegetation for climate change mitigation, *Communications Earth & Environment*, 3, 160, <https://doi.org/10.1038/s43247-022-00489-4>, 2022.
- Hou, Y., Guo, H., Yang, Y., and Liu, W.: Global Evaluation of Runoff Simulation From Climate, Hydrological and Land Surface Models, *Water Resources Research*, 59, e2021WR031817, <https://doi.org/10.1029/2021WR031817>, 2023.
- Huang, H., Liu, J., Chen, A., Ruiz-Vásquez, M., and Orth, R.: State-of-the-art hydrological datasets exhibit low water balance consistency globally, *Earth System Science Data Discussions*, pp. 1–23, <https://doi.org/10.5194/essd-2025-376>, 2025.
- Hurtt, G. C., Chini, L., Sahajpal, R., Frolking, S., Bodirsky, B. L., Calvin, K., Doelman, J. C., Fisk, J., Fujimori, S., Klein Goldewijk, K., Hasegawa, T., Havlik, P., Heinemann, A., Humpenöder, F., Jungclaus, J., Kaplan, J. O., Kennedy, J., Krisztin, T., Lawrence, D., Lawrence, P., Ma, L., Mertz, O., Pongratz, J., Popp, A., Poulter, B., Riahi, K., Shevliakova, E., Stehfest, E., Thornton, P., Tubiello, F. N., van Vuuren, D. P., and Zhang, X.: Harmonization of global land use change and management for the period 850–2100 (LUH2) for CMIP6, *Geoscientific Model Development*, 13, 5425–5464, <https://doi.org/10.5194/gmd-13-5425-2020>, 2020.
- Keenan, T. F., Hollinger, D. Y., Bohrer, G., Dragoni, D., Munger, J. W., Schmid, H. P., and Richardson, A. D.: Increase in forest water-use efficiency as atmospheric carbon dioxide concentrations rise, *Nature*, 499, 324–327, <https://doi.org/10.1038/nature12291>, 2013.
- Knoben, W. J. M., Woods, R. A., and Freer, J. E.: A Quantitative Hydrological Climate Classification Evaluated With Independent Streamflow Data, *Water Resources Research*, 54, 5088–5109, <https://doi.org/10.1029/2018WR022913>, 2018.
- Knutti, R., Furrer, R., Tebaldi, C., Cermak, J., and Meehl, G. A.: Challenges in Combining Projections from Multiple Climate Models, *Journal of Climate*, 23, 2739–2758, <https://doi.org/10.1175/2009JCLI3361.1>, 2010.
- Laimighofer, J., Melcher, M., and Laaha, G.: Parsimonious statistical learning models for low-flow estimation, *Hydrology and Earth System Sciences*, 26, 129–148, <https://doi.org/10.5194/hess-26-129-2022>, 2022.
- Lawrence, D. M., Thornton, P. E., Oleson, K. W., and Bonan, G. B.: The Partitioning of Evapotranspiration into Transpiration, Soil Evaporation, and Canopy Evaporation in a GCM: Impacts on Land–Atmosphere Interaction, *Journal of Hydrometeorology*, 8, 862–880, <https://doi.org/10.1175/JHM596.1>, 2007.
- Leakey, A. D. B., Ainsworth, E. A., Bernacchi, C. J., Rogers, A., Long, S. P., and Ort, D. R.: Elevated CO<sub>2</sub> effects on plant carbon, nitrogen, and water relations: six important lessons from FACE, *Journal of Experimental Botany*, 60, 2859–2876, <https://doi.org/10.1093/jxb/erp096>, 2009.
- Li, C., Zwiers, F., Zhang, X., Li, G., Sun, Y., and Wehner, M.: Changes in Annual Extremes of Daily Temperature and Precipitation in CMIP6 Models, *Journal of Climate*, 34, 3441–3460, <https://doi.org/10.1175/JCLI-D-19-1013.1>, 2021a.
- Li, J., Miao, C., Wei, W., Zhang, G., Hua, L., Chen, Y., and Wang, X.: Evaluation of CMIP6 Global Climate Models for Simulating Land Surface Energy and Water Fluxes During 1979–2014, *Journal of Advances in Modeling Earth Systems*, 13, e2021MS002515, <https://doi.org/10.1029/2021MS002515>, 2021b.
- Lian, X., Piao, S., Chen, A., Huntingford, C., Fu, B., Li, L. Z. X., Huang, J., Sheffield, J., Berg, A. M., Keenan, T. F., McVicar, T. R., Wada, Y., Wang, X., Wang, T., Yang, Y., and Roderick, M. L.: Multifaceted characteristics of dryland aridity changes in a warming world, *Nature Reviews Earth & Environment*, 2, 232–250, <https://doi.org/10.1038/s43017-021-00144-0>, 2021.
- Liao, C., Leung, L. R., Fang, Y., Tesfa, T., and Negron-Juarez, R.: Representing lateral groundwater flow from land to river in Earth system models, *Geoscientific Model Development*, 18, 4601–4624, <https://doi.org/10.5194/gmd-18-4601-2025>, 2025.
- Lovato, T., Peano, D., Butenschön, M., Materia, S., Iovino, D., Scoccimarro, E., Fogli, P. G., Cherchi, A., Bellucci, A., Gualdi, S., Masina, S., and Navarra, A.: CMIP6 Simulations With the CMCC Earth System Model (CMCC-

- ESM2), *Journal of Advances in Modeling Earth Systems*, 14, e2021MS002814, <https://doi.org/10.1029/2021MS002814>, *\_eprint*:  
630 <https://agupubs.onlinelibrary.wiley.com/doi/pdf/10.1029/2021MS002814>, 2022.
- Lundberg, S. M. and Lee, S.-I.: A Unified Approach to Interpreting Model Predictions, *Advances in Neural Information Processing Systems*, 30, <https://doi.org/10.48550/arXiv.1705.07874>, 2017.
- Mankin, J. S., Smerdon, J. E., Cook, B. I., Williams, A. P., and Seager, R.: The Curious Case of Projected Twenty-First-Century Drying but Greening in the American West, *Journal of Climate*, 30, 8689–8710, <https://doi.org/10.1175/JCLI-D-17-0213.1>, 2017.
- 635 Mankin, J. S., Seager, R., Smerdon, J. E., Cook, B. I., Williams, A. P., and Horton, R. M.: Blue Water Trade-Offs With Vegetation in a CO<sub>2</sub>-Enriched Climate, *Geophysical Research Letters*, 45, 3115–3125, <https://doi.org/10.1002/2018GL077051>, 2018.
- Mankin, J. S., Seager, R., Smerdon, J. E., Cook, B. I., and Williams, A. P.: Mid-latitude freshwater availability reduced by projected vegetation responses to climate change, *Nature Geoscience*, 12, 983–988, <https://doi.org/10.1038/s41561-019-0480-x>, 2019.
- Mauritsen, T., Bader, J., Becker, T., Behrens, J., Bittner, M., Brokopf, R., Brovkin, V., Claussen, M., Crueger, T., Esch, M., Fast, I., Fiedler, 640 S., Fläschner, D., Gayler, V., Giorgetta, M., Goll, D. S., Haak, H., Hagemann, S., Hedemann, C., Hohenegger, C., Ilyina, T., Jahns, T., Jimenez-de-la Cuesta, D., Jungclaus, J., Kleinen, T., Kloster, S., Kracher, D., Kinne, S., Kleberg, D., Lasslop, G., Kornbluh, L., Marotzke, J., Matei, D., Meraner, K., Mikolajewicz, U., Modali, K., Möbis, B., Müller, W. A., Nabel, J. E. M. S., Nam, C. C. W., Notz, D., Nyawira, S.-S., Paulsen, H., Peters, K., Pincus, R., Pohlmann, H., Pongratz, J., Popp, M., Raddatz, T. J., Rast, S., Redler, R., Reick, C. H., Rohrschneider, T., Schemann, V., Schmidt, H., Schnur, R., Schulzweida, U., Six, K. D., Stein, L., Stemmler, I., Stevens, B., von 645 Storch, J.-S., Tian, F., Voigt, A., Vrese, P., Wieners, K.-H., Wilkenskjeld, S., Winkler, A., and Roeckner, E.: Developments in the MPI-M Earth System Model version 1.2 (MPI-ESM1.2) and Its Response to Increasing CO<sub>2</sub>, *Journal of Advances in Modeling Earth Systems*, 11, 998–1038, <https://doi.org/10.1029/2018MS001400>, 2019.
- Maxwell, R. M. and Condon, L. E.: Connections between groundwater flow and transpiration partitioning, *Science*, 353, 377–380, <https://doi.org/10.1126/science.aaf7891>, 2016.
- 650 Meyer, H., Reudenbach, C., Wöllauer, S., and Nauss, T.: Importance of spatial predictor variable selection in machine learning applications – Moving from data reproduction to spatial prediction, *Ecological Modelling*, 411, 108815, <https://doi.org/10.1016/j.ecolmodel.2019.108815>, 2019.
- Milly, P. C. D. and Dunne, K. A.: Potential evapotranspiration and continental drying, *Nature Climate Change*, 6, 946–949, <https://doi.org/10.1038/nclimate3046>, 2016.
- 655 Milly, P. C. D. and Dunne, K. A.: Colorado River flow dwindles as warming-driven loss of reflective snow energizes evaporation, *Science*, 367, 1252–1255, <https://doi.org/10.1126/science.aay9187>, 2020.
- Miralles, D. G., Holmes, T. R. H., De Jeu, R. a. M., Gash, J. H., Meesters, A. G. C. A., and Dolman, A. J.: Global land-surface evaporation estimated from satellite-based observations, *Hydrology and Earth System Sciences*, 15, 453–469, <https://doi.org/10.5194/hess-15-453-2011>, 2011.
- 660 Muñoz-Sabater, J., Dutra, E., Agustí-Panareda, A., Albergel, C., Arduini, G., Balsamo, G., Boussetta, S., Choulga, M., Harrigan, S., Hersbach, H., Martens, B., Miralles, D. G., Piles, M., Rodríguez-Fernández, N. J., Zsoter, E., Buontempo, C., and Thépaut, J.-N.: ERA5-Land: a state-of-the-art global reanalysis dataset for land applications, *Earth System Science Data*, 13, 4349–4383, <https://doi.org/10.5194/essd-13-4349-2021>, 2021.
- Nijssen, B., O'Donnell, G. M., Hamlet, A. F., and Lettenmaier, D. P.: Hydrologic Sensitivity of Global Rivers to Climate Change, *Climatic 665 Change*, 50, 143–175, <https://doi.org/10.1023/A:1010616428763>, 2001.

- Niu, G.-Y., Yang, Z.-L., Dickinson, R. E., and Gulden, L. E.: A simple TOPMODEL-based runoff parameterization (SIMTOP) for use in global climate models, *Journal of Geophysical Research: Atmospheres*, 110, <https://doi.org/10.1029/2005JD006111>, 2005.
- Orth, R. and Destouni, G.: Drought reduces blue-water fluxes more strongly than green-water fluxes in Europe, *Nature Communications*, 9, 3602, <https://doi.org/10.1038/s41467-018-06013-7>, 2018.
- 670 Padrón, R. S., Gudmundsson, L., Liu, L., Humphrey, V., and Seneviratne, S. I.: Drivers of intermodel uncertainty in land carbon sink projections, *Biogeosciences*, 19, 5435–5448, <https://doi.org/10.5194/bg-19-5435-2022>, 2022.
- Riahi, K., Van Vuuren, D. P., Kriegler, E., Edmonds, J., O'Neill, B. C., Fujimori, S., Bauer, N., Calvin, K., Dellink, R., Fricko, O., Lutz, W., Popp, A., Cuaresma, J. C., Kc, S., Leimbach, M., Jiang, L., Kram, T., Rao, S., Emmerling, J., Ebi, K., Hasegawa, T., Havlik, P., Humpenöder, F., Da Silva, L. A., Smith, S., Stehfest, E., Bosetti, V., Eom, J., Gernaat, D., Masui, T., Rogelj, J., Strefler, J., Drouet, 675 L., Krey, V., Luderer, G., Harmsen, M., Takahashi, K., Baumstark, L., Doelman, J. C., Kainuma, M., Klimont, Z., Marangoni, G., Lotze-Campen, H., Obersteiner, M., Tabeau, A., and Tavoni, M.: The Shared Socioeconomic Pathways and their energy, land use, and greenhouse gas emissions implications: An overview, *Global Environmental Change*, 42, 153–168, <https://doi.org/10.1016/j.gloenvcha.2016.05.009>, 2017.
- Rockström, J. and Gordon, L.: Assessment of green water flows to sustain major biomes of the world: Implications for future ecohydrological landscape management, *Physics and Chemistry of the Earth, Part B: Hydrology, Oceans and Atmosphere*, 26, 843–851, [https://doi.org/10.1016/S1464-1909\(01\)00096-X](https://doi.org/10.1016/S1464-1909(01)00096-X), 2001.
- Ruehr, S., Keenan, T. F., Williams, C., Zhou, Y., Lu, X., Bastos, A., Canadell, J. G., Prentice, I. C., Sitch, S., and Terrer, C.: Evidence and attribution of the enhanced land carbon sink, *Nature Reviews Earth & Environment*, 4, 518–534, <https://doi.org/10.1038/s43017-023-00456-3>, 2023.
- 685 Scheff, J., Coats, S., and Laguë, M. M.: Why do the Global Warming Responses of Land-Surface Models and Climatic Dryness Metrics Disagree?, *Earth's Future*, 10, e2022EF002814, 2022.
- Schneider, U., Hänsel, S., Finger, P., Rustemeier, E., and Ziese, M.: GPCP Full Data Monthly Product Version 2022 at 1.0°: Monthly Land-Surface Precipitation from Rain-Gauges built on GTS-based and Historical Data, *Deutscher Wetterdienst*, [https://doi.org/10.5676/DWD\\_GPCP/CLIM\\_M\\_V2022\\_100](https://doi.org/10.5676/DWD_GPCP/CLIM_M_V2022_100), 2022.
- 690 Seland, O., Bentsen, M., Olivé, D., Toniazzo, T., Gjermundsen, A., Graff, L. S., Debernard, J. B., Gupta, A. K., He, Y.-C., Kirkevåg, A., Schwinger, J., Tjiputra, J., Aas, K. S., Bethke, I., Fan, Y., Griesfeller, J., Grini, A., Guo, C., Ilicak, M., Karset, I. H. H., Landgren, O., Liakka, J., Moseid, K. O., Nummelin, A., Spensberger, C., Tang, H., Zhang, Z., Heinze, C., Iversen, T., and Schulz, M.: Overview of the Norwegian Earth System Model (NorESM2) and key climate response of CMIP6 DECK, historical, and scenario simulations, *Geoscientific Model Development*, 13, 6165–6200, <https://doi.org/10.5194/gmd-13-6165-2020>, 2020.
- 695 Sellar, A. A., Jones, C. G., Mulcahy, J. P., Tang, Y., Yool, A., Wiltshire, A., O'Connor, F. M., Stringer, M., Hill, R., Palmieri, J., Woodward, S., de Mora, L., Kuhlbrodt, T., Rumbold, S. T., Kelley, D. I., Ellis, R., Johnson, C. E., Walton, J., Abraham, N. L., Andrews, M. B., Andrews, T., Archibald, A. T., Berthou, S., Burke, E., Blockley, E., Carslaw, K., Dalvi, M., Edwards, J., Folberth, G. A., Gedney, N., Griffiths, P. T., Harper, A. B., Hendry, M. A., Hewitt, A. J., Johnson, B., Jones, A., Jones, C. D., Keeble, J., Liddicoat, S., Morgenstern, O., Parker, R. J., Predoi, V., Robertson, E., Siahann, A., Smith, R. S., Swaminathan, R., Woodhouse, M. T., Zeng, G., and Zerroukat, M.: 700 UKESM1: Description and Evaluation of the U.K. Earth System Model, *Journal of Advances in Modeling Earth Systems*, 11, 4513–4558, <https://doi.org/10.1029/2019MS001739>, 2019.

- Seneviratne, S. I., Corti, T., Davin, E. L., Hirschi, M., Jaeger, E. B., Lehner, I., Orlowsky, B., and Teuling, A. J.: Investigating soil moisture–climate interactions in a changing climate: A review, *Earth-Science Reviews*, 99, 125–161, <https://doi.org/10.1016/j.earscirev.2010.02.004>, 2010.
- 705 Singh, N. K., Emanuel, R. E., McGlynn, B. L., and Miniati, C. F.: Soil Moisture Responses to Rainfall: Implications for Runoff Generation, *Water Resources Research*, 57, e2020WR028 827, <https://doi.org/10.1029/2020WR028827>, <https://agupubs.onlinelibrary.wiley.com/doi/pdf/10.1029/2020WR028827>, 2021.
- Skinner, C. B., Poulsen, C. J., Chadwick, R., Diffenbaugh, N. S., and Fiorella, R. P.: The Role of Plant CO<sub>2</sub> Physiological Forcing in Shaping Future Daily-Scale Precipitation, *Journal of Climate*, 30, 2319–2340, <https://doi.org/10.1175/JCLI-D-16-0603.1>, 2017.
- 710 Stein, L., Mukkavilli, S. K., Pfitzmann, B. M., Staar, P. W. J., Ozturk, U., Berrosipi, C., Brunschweiler, T., and Wagener, T.: Wealth Over Woe: Global Biases in Hydro-Hazard Research, *Earth’s Future*, 12, e2024EF004 590, <https://doi.org/10.1029/2024EF004590>, 2024.
- Stigter, E. E., Litt, M., Steiner, J. F., Bonekamp, P. N. J., Shea, J. M., Bierkens, M. F. P., and Immerzeel, W. W.: The Importance of Snow Sublimation on a Himalayan Glacier, *Frontiers in Earth Science*, 6, <https://doi.org/10.3389/feart.2018.00108>, 2018.
- Swann, A. L. S., Hoffman, F. M., Koven, C. D., and Randerson, J. T.: Plant responses to increasing CO<sub>2</sub> reduce estimates of climate impacts on drought severity, *Proceedings of the National Academy of Sciences*, 113, 10 019–10 024, <https://doi.org/10.1073/pnas.1604581113>, 2016.
- 715 Swart, N. C., Cole, J. N. S., Kharin, V. V., Lazare, M., Scinocca, J. F., Gillett, N. P., Anstey, J., Arora, V., Christian, J. R., Hanna, S., Jiao, Y., Lee, W. G., Majaess, F., Saenko, O. A., Seiler, C., Seinen, C., Shao, A., Sigmond, M., Solheim, L., von Salzen, K., Yang, D., and Winter, B.: The Canadian Earth System Model version 5 (CanESM5.0.3), *Geoscientific Model Development*, 12, 4823–4873, <https://doi.org/10.5194/gmd-12-4823-2019>, 2019.
- 720 Séférian, R., Nabat, P., Michou, M., Saint-Martin, D., Voldoire, A., Colin, J., Decharme, B., Delire, C., Berthet, S., Chevallier, M., Sénési, S., Franchisteguy, L., Vial, J., Mallet, M., Joetzer, E., Geoffroy, O., Guérémy, J.-F., Moine, M.-P., Msadek, R., Ribes, A., Rocher, M., Roehrig, R., Salas-y Méliá, D., Sanchez, E., Terray, L., Valcke, S., Waldman, R., Aumont, O., Bopp, L., Deshayes, J., Éthé, C., and Madec, G.: Evaluation of CNRM Earth System Model, CNRM-ESM2-1: Role of Earth System Processes in Present-Day and Future Climate, *Journal of Advances in Modeling Earth Systems*, 11, 4182–4227, <https://doi.org/10.1029/2019MS001791>, 2019.
- 725 Tabari, H.: Climate change impact on flood and extreme precipitation increases with water availability, *Scientific Reports*, 10, 13 768, <https://doi.org/10.1038/s41598-020-70816-2>, 2020.
- Trenberth, K. E.: Changes in precipitation with climate change, *Climate Research*, 47, 123–138, <https://doi.org/10.3354/cr00953>, 2011.
- Ukkola, A. M., Prentice, I. C., Keenan, T. F., van Dijk, A. I. J. M., Viney, N. R., Myneni, R. B., and Bi, J.: Reduced streamflow in water-stressed climates consistent with CO<sub>2</sub> effects on vegetation, *Nature Climate Change*, 6, 75–78, <https://doi.org/10.1038/nclimate2831>, 2016.
- 730 Wada, Y., van Beek, L. P. H., and Bierkens, M. F. P.: Modelling global water stress of the recent past: on the relative importance of trends in water demand and climate variability, *Hydrology and Earth System Sciences*, 15, 3785–3808, <https://doi.org/10.5194/hess-15-3785-2011>, 2011.
- 735 Wada, Y., Flörke, M., Hanasaki, N., Eisner, S., Fischer, G., Tramberend, S., Satoh, Y., van Vliet, M. T. H., Yillia, P., Ringler, C., Burek, P., and Wiberg, D.: Modeling global water use for the 21st century: the Water Futures and Solutions (WFAs) initiative and its approaches, *Geoscientific Model Development*, 9, 175–222, <https://doi.org/10.5194/gmd-9-175-2016>, 2016.
- Wagener, T., Reinecke, R., and Pianosi, F.: On the evaluation of climate change impact models, *WIREs Climate Change*, 13, e772, <https://doi.org/10.1002/wcc.772>, 2022.

- 740 Wei, H., Zhang, Y., Huang, Q., Chiew, F. H. S., Luan, J., Xia, J., and Liu, C.: Direct vegetation response to recent CO<sub>2</sub> rise shows limited effect on global streamflow, *Nature Communications*, 15, 9423, <https://doi.org/10.1038/s41467-024-53879-x>, 2024.
- Weiskel, P. K., Wolock, D. M., Zarrillo, P. J., Vogel, R. M., Levin, S. B., and Lent, R. M.: Hydroclimatic regimes: a distributed water-balance framework for hydrologic assessment, classification, and management, *Hydrology and Earth System Sciences*, 18, 3855–3872, <https://doi.org/10.5194/hess-18-3855-2014>, 2014.
- 745 Wu, T., Lu, Y., Fang, Y., Xin, X., Li, L., Li, W., Jie, W., Zhang, J., Liu, Y., Zhang, L., Zhang, F., Zhang, Y., Wu, F., Li, J., Chu, M., Wang, Z., Shi, X., Liu, X., Wei, M., Huang, A., Zhang, Y., and Liu, X.: The Beijing Climate Center Climate System Model (BCC-CSM): the main progress from CMIP5 to CMIP6, *Geoscientific Model Development*, 12, 1573–1600, <https://doi.org/10.5194/gmd-12-1573-2019>, 2019.
- Yang, H., Piao, S., Huntingford, C., Ciais, P., Li, Y., Wang, T., Peng, S., Yang, Y., Yang, D., and Chang, J.: Changing the retention properties of catchments and their influence on runoff under climate change, *Environmental Research Letters*, 13, 094019, <https://doi.org/10.1088/1748-9326/aadd32>, 2018.
- 750 Yang, Y., McVicar, T. R., Yang, D., Zhang, Y., Piao, S., Peng, S., and Beck, H. E.: Low and contrasting impacts of vegetation CO<sub>2</sub> fertilization on global terrestrial runoff over 1982–2010: accounting for aboveground and belowground vegetation–CO<sub>2</sub> effects, *Hydrology and Earth System Sciences*, 25, 3411–3427, <https://doi.org/10.5194/hess-25-3411-2021>, 2021.
- Yang, Y., Roderick, M. L., Guo, H., Miralles, D. G., Zhang, L., Fatichi, S., Luo, X., Zhang, Y., McVicar, T. R., Tu, Z., Keenan, T. F., Fisher, J. B., Gan, R., Zhang, X., Piao, S., Zhang, B., and Yang, D.: Evapotranspiration on a greening Earth, *Nature Reviews Earth & Environment*, 4, 626–641, <https://doi.org/10.1038/s43017-023-00464-3>, 2023.
- 755 Yin, J., Gentile, P., Zhou, S., Sullivan, S. C., Wang, R., Zhang, Y., and Guo, S.: Large increase in global storm runoff extremes driven by climate and anthropogenic changes, *Nature Communications*, 9, 4389, <https://doi.org/10.1038/s41467-018-06765-2>, 2018.
- Young, A. M., Friedl, M. A., Novick, K., Scott, R. L., Moon, M., Frohking, S., Li, X., Carrillo, C. M., and Richardson, A. D.: Disentangling the Relative Drivers of Seasonal Evapotranspiration Across a Continental-Scale Aridity Gradient, *Journal of Geophysical Research: Biogeosciences*, 127, e2022JG006916, <https://doi.org/10.1029/2022JG006916>, <https://agupubs.onlinelibrary.wiley.com/doi/pdf/10.1029/2022JG006916>, 2022.
- 760 Zaitchik, B. F., Rodell, M., Biasutti, M., and Seneviratne, S. I.: Wetting and drying trends under climate change, *Nature Water*, 1, 502–513, <https://doi.org/10.1038/s44221-023-00073-w>, 2023.
- 765 Zhao, Q., Zhu, Z., Zeng, H., Zhao, W., and Myneni, R. B.: Future greening of the Earth may not be as large as previously predicted, *Agricultural and Forest Meteorology*, 292–293, 108–111, <https://doi.org/10.1016/j.agrformet.2020.108111>, 2020.
- Zheng, H., Yang, Z.-L., Lin, P., Wei, J., Wu, W.-Y., Li, L., Zhao, L., and Wang, S.: On the Sensitivity of the Precipitation Partitioning Into Evapotranspiration and Runoff in Land Surface Parameterizations, *Water Resources Research*, 55, 95–111, <https://doi.org/10.1029/2017WR022236>, 2019.
- 770 Zhu, Z., Piao, S., Myneni, R. B., Huang, M., Zeng, Z., Canadell, J. G., Ciais, P., Sitch, S., Friedlingstein, P., Arneth, A., Cao, C., Cheng, L., Kato, E., Koven, C., Li, Y., Lian, X., Liu, Y., Liu, R., Mao, J., Pan, Y., Peng, S., Peñuelas, J., Poulter, B., Pugh, T. A. M., Stocker, B. D., Viovy, N., Wang, X., Wang, Y., Xiao, Z., Yang, H., Zaehle, S., and Zeng, N.: Greening of the Earth and its drivers, *Nature Climate Change*, 6, 791–795, <https://doi.org/10.1038/nclimate3004>, 2016.